



HAL
open science

Multiple subtropical stratospheric intrusions over Reunion Island: Observational, Lagrangian, and Eulerian numerical modeling approaches

Hélène Vérèmes, Jean-Pierre Cammas, Jean-Luc Baray, Philippe Keckhut, Christelle Barthe, Françoise Posny, Pierre Tulet, Davide Dionisi, Soline Bielli

► **To cite this version:**

Hélène Vérèmes, Jean-Pierre Cammas, Jean-Luc Baray, Philippe Keckhut, Christelle Barthe, et al.. Multiple subtropical stratospheric intrusions over Reunion Island: Observational, Lagrangian, and Eulerian numerical modeling approaches. *Journal of Geophysical Research: Atmospheres*, 2016, 121 (24), pp.14,414-14,432. 10.1002/2016JD025330 . hal-01449884

HAL Id: hal-01449884

<https://hal.science/hal-01449884>

Submitted on 28 Jun 2018

HAL is a multi-disciplinary open access archive for the deposit and dissemination of scientific research documents, whether they are published or not. The documents may come from teaching and research institutions in France or abroad, or from public or private research centers.

L'archive ouverte pluridisciplinaire **HAL**, est destinée au dépôt et à la diffusion de documents scientifiques de niveau recherche, publiés ou non, émanant des établissements d'enseignement et de recherche français ou étrangers, des laboratoires publics ou privés.

RESEARCH ARTICLE

10.1002/2016JD025330

Key Points:

- Ozone and water vapor lidar observations of a multiple stratospheric intrusion events over Reunion Island
- Reconstruction of the 3-D structures of stratospheric air masses in the upper troposphere
- Eulerian and Lagrangian models' ability to simulate realistically a multiple stratospheric intrusions process

Correspondence to:

H. Vérémes,
helene.veremes@univ-reunion.fr

Citation:

Vérémes, H., J.-P. Cammas, J.-L. Baray, P. Keckhut, C. Barthe, F. Posny, P. Tulet, D. Dionisi, and S. Bielli (2016), Multiple subtropical stratospheric intrusions over Reunion Island: Observational, Lagrangian, and Eulerian numerical modeling approaches, *J. Geophys. Res. Atmos.*, 121, 14,414–14,432, doi:10.1002/2016JD025330.






Received 7 MAY 2016

Accepted 30 NOV 2016

Accepted article online 6 DEC 2016

Published online 22 DEC 2016

Multiple subtropical stratospheric intrusions over Reunion Island: Observational, Lagrangian, and Eulerian numerical modeling approaches

H. Vérémes^{1,2} , J.-P. Cammas^{1,2} , J.-L. Baray³, P. Keckhut⁴, C. Barthe¹ , F. Posny¹, P. Tulet¹ , D. Dionisi⁵ , and S. Bielli¹

¹Laboratoire de l'Atmosphère et des Cyclones, UMR 8105, CNRS-Université de la Réunion-Météo-France, Saint Denis de la Réunion, France, ²Observatoire des Sciences de l'Univers de La Réunion, UMS 3365, CNRS-Université de la Réunion, Saint Denis de la Réunion, France, ³Laboratoire de Météorologie Physique, UMR 6016, CNRS-Observatoire de Physique du Globe de Clermont-Ferrand, CNRS-Université Blaise Pascal, Clermont-Ferrand, France, ⁴Laboratoire Atmosphères, Milieux, Observations Spatiales - IPSL, UMR 8190, CNRS-UVSQ-UPMC, UniverSud Paris, Guyancourt, France, ⁵Institute for Atmospheric Sciences and Climate, National Research Council (CNR), Rome, Italy

Abstract Signatures of multiple stratospheric intrusions were observed on simultaneous and collocated ozone and water vapor profiles retrieved by lidars and radiosondes at the Maïdo Observatory, Reunion Island (21°S, 55°E, 2160 m above sea level), during MAïdo Lidar Calibration CAmpaign in April 2013. A singular structure of the ozone vertical profile with three peaks (in excess of 90 ppbv, at ~8, ~10, and ~13 km altitude) embedded in a thick dry layer of air suggested stratospheric intrusions with multiple origins. The hypothesis is corroborated by a synoptic analysis based on re-analyses. European Centre for Medium-Range Weather Forecasts ERA-Interim temporal series associated with 5 days Lagrangian back trajectories initialized on each ozone peak allows to capture their stratospheric origin. The ozone peak at the lowest altitude is associated with an irreversible tropopause folding process along the polar jet stream during an extratropical cutoff low formation. Simultaneous lidar water vapor profiles of this peak show that the anticorrelation with ozone has been removed, due to mixing processes. Back trajectories indicate that the two other ozone peaks observed at higher altitudes are associated with the dynamics of the subtropical jet stream and the lower stratosphere. The observations confirm the recent stratospheric origins. The highest ozone peak is explained by the horizontal distribution of the intrusion. Use of a Lagrangian Reverse Domain Filling model and of the Meso-NH Eulerian mesoscale model with a passive stratospheric tracer allow to further document the stratosphere-troposphere transport processes and to describe the detailed potential vorticity and ozone structures in which are embedded in the observed multiple stratospheric intrusions.

1. Introduction

In the context of global climate change, it is very important to survey stratosphere-troposphere exchanges (STE) to understand these dynamical processes and to improve their representation in numerical weather prediction and climate models. STE processes are crucial because both radiative and oxidizing roles of ozone depend on its vertical distribution in the troposphere and in the stratosphere [Schwarzkopf and Ramaswamy, 1993; Kley, 1997]. Global aspects of STE in the framework of the general circulation, including the role of waves, eddies, and mesoscale structures such as jet streams and extratropical cyclone dynamics, have been the subject of a review by Holton *et al.* [1995]. Several studies focused on STE associated with synoptic-scale jet stream and Rossby wave dynamics [e.g., Ancellet *et al.*, 1994; Postel and Hitchman, 1999; Scott *et al.*, 2001; Scott and Cammas, 2002; Baray *et al.*, 2000, 2003], jet-front dynamics [Donnadille *et al.*, 2001; Flentje *et al.*, 2005], and tropical cyclones [Das *et al.*, 2011; Leclair de Bellevue *et al.*, 2006]. Most of the case studies on stratospheric intrusions conclude that a part of this exchange is irreversible and impacts the tropospheric ozone budget [e.g., Collins *et al.*, 2003; Cristofanelli *et al.*, 2006; Hess and Zbinden, 2013; Roelofs and Lelieveld, 2000]. Even if the tropospheric ozone budget derived from chemistry transport global models reasonably agrees with ozone observations, the representations of the three main drivers of the budget—photochemistry (productions and losses), dry deposit on the surface, and STE—and a right balance between them need further improvement [Stevenson *et al.*, 2006, 2013]. Thus, it is important to document those processes including stratospheric intrusions to better evaluate the ozone fluxes and budget.

Depending on a mechanism of tropopause folding [Reed, 1955; Reed and Danielsen, 1958], a stratospheric intrusion is characterized as stratospheric air masses subsiding isentropically within tropopause folds associated with the creation of tongues of ozone-rich and dry air in the troposphere [Appenzeller and Davies, 1992; Holton et al., 1995]. Parameters like potential vorticity [Appenzeller and Davies, 1992; Danielsen, 1968; Danielsen et al., 1970; Reed and Danielsen, 1958], ozone [Danielsen, 1968], and water vapor [Shapiro, 1978] concentrations, with different orders of magnitude between the stratosphere and the troposphere, are relatively well conserved [Appenzeller et al., 1996] and are correlated [Danielsen et al., 1970, Shapiro, 1974] during tropopause foldings. Newell et al. [1999] showed that by taking simple detection criteria on the O_3/H_2O relationship, different type of air masses could be differentiated. For an O_3+H_2O relationship (i.e., anticorrelation), the air mass was identified as stratospheric air or pollution. Mixing of the stratospheric parcel with the wet tropospheric air [Stohl et al., 2003a] can explain that the analysis of the relative humidity as a tracer is not always conclusive and mainly explains why the anticorrelation O_3/H_2O is not always sufficient to reliably characterize layers associated to stratospheric intrusions [Colette et al., 2005; Thouret et al., 2000]. A dynamical parameter, the potential vorticity (PV), is used as a tracer of STE. Under adiabatic and frictionless conditions, PV is conserved on isentropic surfaces and is a parameter well adapted to study dynamic processes such as tropopause folds and stratospheric intrusions [Reed and Danielsen, 1958; Hoskins et al., 1985]. These three tracers are the best parameters and can be used in different methodologies to identify and characterize stratospheric intrusions. The first approach to study is instrumental. High-resolution in situ or remote sensing measurements are mainly used to sample stratospheric filaments. Recent research works on the O_3/H_2O relationship focused on high-resolution data like water vapor ground-based lidar measurements to study stratospheric intrusions [D'Aulerio et al., 2005]. The optimal data set should be co-localized and coincident measures. The Measurements of Humidity in the Atmosphere and Validation Experiments campaign led to ozone and water vapor coupled lidar observations of a stratospheric intrusion at the Table Mountain Facility in 2009 [Leblanc et al., 2011]. Another approach to document such processes consists in describing the synoptic analysis of the event, thanks to global model (re-)analyses, such as, for example, for this case study the ones from ECMWF (European Centre for Medium-Range Weather Forecasts). ECMWF analyses contain all parameters allowing the characterization of a stratospheric intrusion [Vaughan et al., 1994] and especially the potential vorticity which is not directly measured. More than characterizing a single event, those global analyses data have been and are still largely used to establish climatologies [Škerlak et al., 2014, 2015; Sprenger and Wernli, 2003; Sprenger et al., 2007] and to calculate exchanges induced by STE (including stratospheric intrusions). Finally, to go further in the investigations, high-resolution modeling is the preferred method. On the one hand, Lagrangian calculations can reveal subgrid scale structures [e.g., Stohl et al., 2003a; Trickl et al., 2010] where transport dominates and are, thus, well adapted. A few case studies of stratospheric intrusions have already been evaluated with Lagrangian tools, like the LAGRangian ANalysis TOol [Wernli and Davies, 1997; Wernli, 1997], the Hybrid Single Particle Lagrangian Integrated Trajectory model [Draxler and Hess, 1998], or the FLEXible PARTicle dispersion model [Stohl et al., 1998, 2005; Stohl and Trickl, 1999]. On the other hand, previous studies have shown that mesoscale modeling could be used as an integrating tool for studying and/or quantifying transport processes especially in the upper troposphere-lower stratosphere [Cristofanelli et al., 2003; Ebel et al., 1991; Kentarchos et al., 1999; Leclair de Bellevue et al., 2007; Luo et al., 2013; Meloan et al., 2003]. To establish climatologies, ECMWF analyses are often coupled with Lagrangian calculations [Bourqui, 2006; Bourqui et al., 2012; Cristofanelli et al., 2006; Sprenger et al., 2003]. Coupled to ECMWF forecasts, some Lagrangian tools can also guide some measurement campaigns [Trickl et al., 2010; Zanis et al., 2003] as the STACCATO one (Influence of Stratosphere-Troposphere Exchange in a Changing Climate on Atmospheric Transport and Oxidation Capacity) [Stohl et al., 2003b]. The different data and methodologies described in this introduction might be coupled to establish the best diagnostic of a stratospheric intrusion process.

Until now, very few STE case studies focused on the Southern Hemisphere mainly because of the lack of high-resolution measurements which require in situ and remote sensing instruments. Using the ozonesonde data of the NDACC/SHADOZ station (Network for the Detection of Atmospheric Composition Change/Southern Hemisphere ADDitional OZonesondes), some studies have been published on ozone aspects in STE on the southwestern part of the Indian Ocean [Baray et al., 1998, 2000; Leclair De Bellevue et al., 2007; Clain et al., 2010]. Reunion Island (21°S, 55.5°E) is located on a subtropical latitude band of the Southern Hemisphere. The latitude of the island allows observations of different thermodynamic processes depending on the season, e.g., processes associated with the Intertropical Convergence Zone during its poleward migration in

austral summer or the processes associated with the upper tropospheric jet streams during their equatorward migration in boreal winter. Its position makes possible observations of tropical and subtropical mechanisms. It is also a strategic location to monitor climate change, considering the widening of the tropical belt [Lu *et al.*, 2009]. The Maïdo Observatory, a high altitude site, is equipped with various in situ and remote sensing instruments [Baray *et al.*, 2013]. The different collocated lidars of the observatory provide high-resolution profiles of water vapor, ozone, and aerosols which represent an original data set to document STE studies. The MALICCA (MAïdo Lidar Calibration CAmpaign) field campaign conducted in April 2013 [Keckhut *et al.*, 2015] has provided an important water vapor and ozone profiles and column data set. The objective of this paper is to analyze in detail an event of multiple stratospheric intrusions observed between 28 March and 5 April 2013 in ozone lidar profiles, in water vapor lidar, and radiosounding profiles. A main goal is to explain the multilayered nature of the stratospheric intrusions observed over Reunion Island with respect to the dynamics of the subtropical and polar jet streams. Another goal is to investigate the relationship in the subtropics between ozone and water vapor within the stratospheric intrusions as it is described by lidar and sonde observations. The multi-instrumented lidar measurements and numerical approaches, Lagrangian and mesoscale models, will allow to bring new characterization elements regarding the history of the stratospheric intrusions. In section 2, we describe the measurement site and the methodology. Section 3 focuses on the synoptic characterization of the stratospheric intrusion and on the differentiation of the air masses. The history of each ozone peak is reconstituted, thanks to the observations and the modeling results. The reliability of measurements and the complementarity and/or limits of the different methodological approaches are also discussed. Finally, conclusion is set in section 4.

2. Instrumentation and Methodology

2.1. Instrumentation

2.1.1. The Maïdo Observatory

Atmospheric ozone measurement systems have been deployed at Reunion Island since the nineties, beginning with radiosoundings, followed by a *Système d'Analyse par Observation Zénithale* UV-visible spectrometer [Pommereau and Goutail, 1988] and lidar systems. Reunion Island represents a prime location because there are very few multi-instrumented stations in the tropics and particularly in the Southern Hemisphere. In 2012, the Maïdo Observatory (2160 m above sea level (asl)) was commissioned on the western part of the island. It hosts various instruments for atmospheric measurements, including lidar systems, spectroradiometers, and in situ gas and aerosol measurements [Baray *et al.*, 2013].

During the night, clear-sky conditions are favored at the observatory due to large-scale subtropical and anticyclonic subsidence which is reinforced by local conditions on the downstream side of the island. In April, the Mascarene subtropical high strongly influences the meteorology over Reunion Island. Under this large-scale feature and on the lee side of the island, the synoptic subsidence is locally reinforced by the downslope flow [Lesouëf *et al.*, 2011]. Air masses at the Maïdo site are separated from local and regional sources of pollution at nighttime, and the performances of the optical instruments above the marine boundary layer have been considerably improved [Baray *et al.*, 2013].

The intensive measurement campaign MALICCA-1 (1 April to 20 April 2013) provided detailed data set of water vapor profiles on a short period. The main goal of the campaign was to set the best instrumental configuration for the Raman lidar system and to evaluate its data [Dionisi *et al.*, 2015; Keckhut *et al.*, 2015]. This campaign allowed also to conduct scientific studies on various topics: moistening of the lower stratosphere, cirrus clouds, among others, and STE including the case study documented in this paper.

2.1.2. The Tropospheric Ozone Lidar

A Rayleigh-Mie lidar has been deployed at Saint-Denis (north of Reunion Island) and was performing several times a week since 1998 [Baray *et al.*, 2006]. This system has been upgraded and transferred to the Maïdo station in 2012 [Baray *et al.*, 2013]. This lidar is a differential absorption lidar system: profiles are retrieved from the differential absorption in air of two wavelengths (289 and 316 nm). For the emission part, the UV wavelengths are generated by Raman shifting of the fourth harmonic of a neodymium: yttrium/aluminum/garnet (Nd:YAG) laser in a high-pressure deuterium cell [Baray *et al.*, 1999]. The laser frequency is 30 Hz. The beam diameter is 10 mm and is expanded in a divergence optimizer system located after the Raman cell (length and diameter in/out, respectively: 1500, 20, and 55 mm). The output diameter and the divergence of the emitted beam are 30 mm and 0.25 mrad [Baray *et al.*, 2013]. The reception part of the system is composed

of a mosaic of four telescopes (500 mm diameter each) and optical fibers (1.5 mm diameter), and the spectral separation of 289 and 316 nm beams is operated by a spectrometer (with a Czerny-Turner holographic grating).

First ozone measurements at the Maïdo were performed in January 2013. The lower and upper limits of the validity are 5–6 km to 16–18 km asl, respectively, depending on meteorological conditions and on the quality of the signal. To keep the lower limit for the vertical range of the measurements to 3–4 km asl, a low channel (small telescope of 20 cm diameter) has been added to the setup of the lidar at the Maïdo Observatory. A commutation allows to work with either mode by permuting the optical fibers at the entrance of the spectrometer. The data processing is described in *Baray et al.* [1999]. Routinely, measurements are performed on average 5 times by month at the Maïdo station. The vertical resolution is approximately 400 m at 8 km asl and 1.2 km at 14 km asl.

2.1.3. The Water Vapor Lidar

The Raman water vapor lidar system which operated at Saint-Denis from 2002 to 2005 [*Hoareau et al.*, 2012] has been very significantly upgraded after being transferred to the Maïdo station in 2012. Some critical points detected in the previous system have been improved and optimized [*Hoareau et al.*, 2012; *Dionisi et al.*, 2015]. The new Raman system has been designed to monitor the water vapor in the troposphere and in the lower stratosphere and, simultaneously, the temperature in the stratosphere and in the mesosphere. The new lidar system uses the 355 nm, generated by two Nd:YAG lasers, with a repetition rate of 30 Hz. Even if the system has been designed to work at two wavelengths, only the 355 nm wavelength is used on a routine basis. Emitting pulses of each laser are synchronized and coupled through a polarization cube, have an energy of 375 mJ per pulse and a duration pulse of 9 ns. The geometric divergence of the beam is around 0.5 mrad. One of the specificities of this lidar configuration is the coaxial geometry for emission and reception designed to avoid parallax effects, extend measurement down to the ground, and facilitate the optical alignment and the calibration procedure. Another specificity is that the backscattered signal (collected by a 1.2 m diameter telescope) is transferred to the optical part by a set of lenses and mirrors instead of fiber-optic cables. The fluorescence in fiber-optic cables could cause a systematic bias in water vapor measurements [*Sherlock et al.*, 1999] that is avoided with the new design. The field of view of the system is set to 0.5 mrad (2 mm), thanks to a diaphragm field stop at the entrance of this box to avoid the saturation of the detectors due to the defocalization effect. The spectral separation of the light is realized by dichroic beam splitters and band-pass and high-pass interference filters. Details on the optical configuration are given in *Dionisi et al.* [2015]. Photons are counted by using Hamamatsu photomultiplier with Licel transient recorders [*Hoareau et al.*, 2012]. Water vapor profiles are retrieved by using the method described in *Dionisi et al.* [2015]. Long-term calibration is performed by using water vapor columns obtained from Global Navigation Satellite Systems (GNSS). The GNSS data are collocated and simultaneous with the Raman lidar measurements. At the Maïdo Observatory, lidar measurements are routinely performed twice a week on average. The vertical resolution of the raw data is 15 m. On a routine basis, data are smoothed with a Blackman filter whose number of points changes with the altitude. The method of calculation of the vertical resolution is based on *Leblanc et al.* [2016] and retrieves values around 100 m at 4 km asl, 250 m at 12.5 km asl, 300 m at 15 km asl, and 375 m at 18 km asl.

2.1.4. Radiosoundings

PTU (pressure-temperature-humidity) radiosondes were launched from the Maïdo Observatory site during MALICCA-1 [*Keckhut et al.*, 2015]: 12 Modem M10 radiosoundings and 15 Vaisala RS92 radiosoundings, including four dualflights (Modem and Vaisala) launched simultaneously to the beginning of the water vapor lidar shots. The main objectives in performing those specific measurements were, with the dualflights, a comparison between different types of PTU radiosonde data, a comparison of the use of radiosoundings versus GPS for the calibration of the water vapor lidar [*Dionisi et al.*, 2015], and a multi-instrumented comparison in order to validate the Raman water vapor measurements. Biases of the Modem M10 sensors are known and are being the subject of corrections in order to fit the GRUAN (Global Climate Observing System Reference Upper-Air Network) framework requirements (work in progress at the MeteoModem company; G. Clain personal communication). The Modem M10 data of MALICCA used in this paper benefited of corrections on response time and heating of the sensors that were not yet implemented in the code in April 2013.

2.2. Numerical Modeling

2.2.1. Operational Analysis and ERA-Interim Re-Analysis

The analysis of the synoptic context is based on the interpretation of ERA-Interim re-analyses [*Berrisford et al.*, 2011]. Vertical and horizontal resolutions of the parameters extracted (ozone, potential vorticity, water

Table 1. Description of the Different Types of ECMWF Data Used in the Present Study

| Method | Synoptic Analysis | LACYTRAJ | Meso-NH |
|-----------------------|-------------------|-------------|-------------|
| ECMWF data | ERA-Interim | ERA-Interim | Operational |
| Temporal resolution | 6 h | 6 h | 6 h |
| Type of level | Pressure | Pressure | Model |
| Number of levels | 37 | 37 | 60 |
| Horizontal resolution | 0.5° | 0.75° | 0.5° |

threshold [Holton *et al.*, 1995 ; Hoskins *et al.*, 1985] as the iso-surface -2 PVU (potential vorticity unit = $10^{-6} \text{ km}^2 \text{ kg}^{-1} \text{ s}^{-1}$) is more appropriate in our study. Ozone is a prognostic variable predicted simultaneously with the other model state variables in the 4D-Var ERA-Interim assimilation scheme [Dee *et al.*, 2011]. The ozone first guess is derived from an updated version of the Cariolle and Déqué [1986] scheme [Cariolle and Teysseire, 2007].

2.2.2. LACYTRAJ

LACYTRAJ is a kinematic trajectory code using the ECMWF operational analyses or ERA-Interim re-analyses. The user defines a start grid (either a 1-D vertical profile or a 2-D vertical/horizontal cross section), and particles (or air masses) positioned over model grid point are advected by 3-D analyzed wind components. The altitude of the particles is computed by using the vertical component of the wind of ECMWF operational analyses or ERA-Interim re-analyses. Tracers can be advected along trajectories, in order to rebuild an advected parameter's profile or field. This technique, known as Reverse Domain Filling, hereafter RDF [Sutton *et al.*, 1994], allows to retrieve subgrid-scale information when the time step of the trajectory is adjusted to the lifetime of the parameter and assuming that no mixing process takes place along this path. This Lagrangian technique has been used with various trajectory models to study the dynamics of the polar vortex and the formation of filaments along its edge [Schoeberl and Newman, 1995], to trace troposphere-to-stratosphere transport above a midlatitude deep convective system [Hegglin *et al.*, 2004], to identify the water vapor transport pathways over the summertime Asian monsoon region [Zhang *et al.*, 2016], to construct a three-dimensional gridded climatology of ozone [Liu *et al.*, 2013], etc. The LACYTRAJ model has been developed to investigate STE, either in case studies [Baray *et al.*, 2010, 2012; Clain *et al.*, 2010] or for climatologies [Clain *et al.*, 2010].

For the present study, 5 day back trajectories have been calculated from atmospheric columns on the closest grid points to Reunion Island initialized with the ECMWF re-analyses of 4 April at 1800 UTC (Table 1), with a time step of 15 min and a pressure step (i.e., the vertical spacing of the starting positions) of 10 to 50 hPa depending on the altitude. Furthermore, subgrid structures are reconstructed by using the RDF method by advecting the ozone and the potential vorticity from 1 to 7 days, with a time step of 15 min and a vertical spacing of 5 hPa on a space domain from 5 to 30°S and 40 to 85°E. The time horizon of the RDF analysis, constructed with back trajectories and initially extended up to 7 days, was finally set at 2 days. The mean reason for this is twofold: (i) the period of time needed for the air particles to irreversibly cross the tropopause is linked to the typical duration of a Rossby wave breaking (RWB) event (i.e., 2 to 3 days) and (ii) the RWB event occurred just upstream of and over Reunion Island (see section 3.1); thus, the air particles did not take much time to reach the point of observation. We noted that no additional relevant information was provided extending the time range beyond 2 days. On the contrary even, a gradual increase of both the noise of the advected fields and the disappearance of fine-scale upper level features takes shape as the time range increases. Moreover, the model assuming that there is no mixing process along the trajectory, the RDF approach will bring some information about the maximum possible ozone concentration at the target position.

2.3.3. Meso-NH

Meso-NH is a nonhydrostatic research model [Lafore *et al.*, 1998]. It is used herein to describe the fine-scale dynamics associated with tropopause folds, as already done for extratropical [Donnadille *et al.*, 2001; Tulet *et al.*, 2002] and for tropical case studies [Leclair de Bellevue *et al.*, 2007; Scott *et al.*, 2001].

The case study is simulated with one model with a horizontal grid spacing of 24 km. The vertical grid has 150 vertical levels with 150 m grid spacing (from the 1 to 21 km). A sponge layer is applied from 18 to 21 km in order to dampen the upward propagating gravity waves generated by the convection. The horizontal

vapor mixing ratio, and wind) are given in Table 1. The thermal definition of the tropopause [World Meteorological Organization, 1986] can fail in representing the dynamical situation associated with a tropopause fold [Kuang *et al.*, 2012]. The dynamical definition based on a potential vorticity

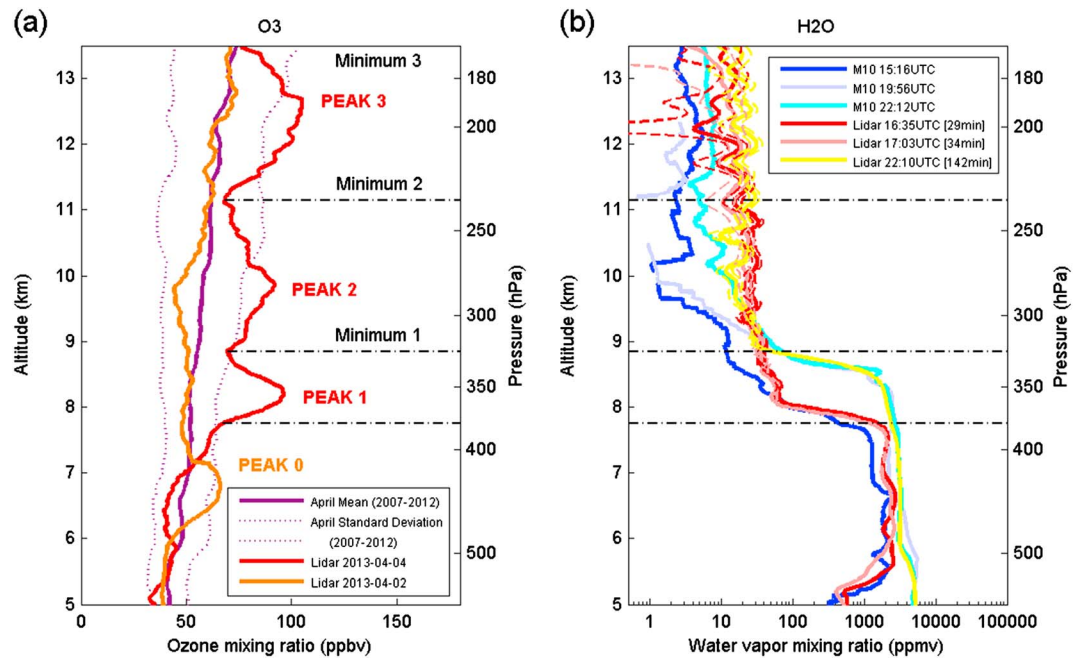


Figure 1. (a) Lidar profiles of ozone mixing ratio (in ppbv) at the Mado Observatory on 4 April 2013 at 1610 UTC (red) and 2 April 2013 at 2151 UTC (orange). The ozone average profile for a month of April and its standard deviation derived from the 2007–2012 weekly NDACC/SHADOZ radiosounding database at Reunion station are displayed with a purple solid and dotted line, respectively. (b) Lidar profiles of water vapor mixing ratio (in ppmv) at the Mado Observatory and their 1σ error for 4 April 2013 at 1635 UTC (red solid and dotted lines), at 1703 UTC (pink solid and dotted lines), and at 2210 UTC (yellow solid and dotted lines, respectively) and Modem water vapor radiosounding profiles on 4 April 2013 at 1516 UTC (blue line) and at 1956 UTC (sky blue line) and at 2212 UTC (cyan line).

domain covers the South West Indian Ocean region with an area of about $4320 \text{ km} \times 4800 \text{ km}$ (180×200 points). The time step is 15 s. The simulation is integrated from 0000 UTC on 2 April 2013 to 1800 UTC on 5 April 2013. The initial and lateral boundary conditions are obtained from European Centre for Medium-Range Weather Forecast (ECMWF) operational analyses.

The physics of the model includes the prognostic calculation of turbulence following *Bougeault and Lacarrère* [1989]. A convection scheme based on mass-flux calculations is used [*Bechtold et al., 2001*]. Mixed-phase microphysics [*Pinty and Jabouille, 1998*] and subgrid cloudiness [*Chaboureau and Bechtold, 2005*] are used for these simulations. The Rapid Radiation Transfer Model scheme of ECMWF is used for radiation [*Mlawer et al., 1997*]. A new scalar variable has been implemented in Meso-NH: a stratospheric ozone tracer. In order to initialize this variable, the ozone is extracted from the ozone parameter of the CAMS (Copernicus Atmosphere Monitoring Service) near real-time analyses [*Inness et al., 2009*]. Tracer values are set to zero wherever the CAMS ozone parameter is below a stratospheric threshold. This method allows to take account of the stratospheric-origin air initially present in the troposphere and entering it through the boundaries of the domain during the model run. Setting to zero the tracer below the stratospheric threshold avoids confusing stratospheric-origin air being mixed in the troposphere with the background tropospheric ozone. Some sensitivity tests have been performed in order to choose the best starting date, vertical resolution, altitude of the beginning of the sponge layer, and threshold for the stratospheric ozone. The sensitivity tests were conclusive when the comparisons of Meso-NH fields were in agreement with the 4 April ozone lidar profile (Figure 1) or with the advected PV and ozone cross sections (see section 3.2). The result of the test shows that the most suitable threshold for the stratospheric ozone tracer is 70 ppbv. On the observations, this altitude is representative of the ozone tropospheric background: it corresponds to the highest amount of ozone in the troposphere for which the lidar profile on 4 April and the climatological profile of ozone for a month of April are in agreement. When looking at the ECMWF ERA-Interim re-analyses, the 70 ppbv contour seems significant, highlighting a structure from the ozone background (see section 3.2).

Table 2. Measurements at the Maïdo Observatory on 2 and 4 April 2013 (MALICCA-1)

| Date | 2 April 2013 | | 4 April 2013 | | |
|-----------------|--------------------------|--------------------|----------------------------|----------------------------|--------------------|
| Parameter | Water vapor mixing ratio | Ozone mixing ratio | Water vapor mixing ratio | Water vapor mixing ratio | Ozone mixing ratio |
| Instrument | Radiosonde (M10) | Lidar | Radiosonde (M10) | Lidar | Lidar |
| Type of product | Profile | Integrated profile | Profile | Integrated profile | Integrated profile |
| Launch time | 1600 UTC 2157 UTC | 2151 UTC | 1535 UTC 1956 UTC 2212 UTC | 1635 UTC 1703 UTC 2210 UTC | 1610 UTC |

3. Characterization of the Stratospheric Intrusions

3.1. Ozone-Rich and Dry Layers in the Upper Troposphere

Figure 1 shows the lidar ozone profiles on 2 April 2013 at 2151 UTC and 4 April at 1610 UTC and the different lidar and radiosounding water vapor profiles on 4 April 2013 at 1516 UTC and 5 April at 0032 UTC. On the ozone lidar profile measured 2 days before (2 April 2013, see the orange line on Figure 1a), a small peak is observed (60 ppbv) at a low altitude (6.8 km). With regards to ozone observations (Table 2), the lidar vertical profile on 4 April (Figure 1a, red line) shows three distinct peaks at 8.2, 9.9, and 12.7 km altitude with ozone mixing ratios of 97 ppbv (peak no. 1), 92 ppbv (peak no. 2), and 105 ppbv (peak no. 3), respectively. Above the tropopause at 16 km altitude, stratospheric standard values of ozone are observed by the lidar (not shown). All these tropospheric ozone peaks can be considered as significant positive anomalies of ozone when they are compared to the mean April ozone profile derived from 158 weekly NDACC-SHADOZ radiosoundings between 2007 and 2012 (Figure 1a, purple line). The Meteosat water vapor image on 4 April 2013 at 1800 UTC (Figure 2) shows a synoptic and very dry upper tropospheric trough extending equatorward and just west of Reunion Island. All available lidar and radiosonde water vapor vertical profiles on 4 April (Figure 1b and Table 1) also show that a very dry air mass with concentrations below 100 ppmv is in place above 9 km altitude. Compared with the mean water vapor profile derived with all lidar observations obtained during the MALICCA-1 campaign (see Figure 12 in *Dionisi et al.* [2015]), this very dry air mass can be considered as an anomalous pattern of dryness in the middle and upper troposphere.

The observations of very dry and ozone-rich layers exceeding the ozone climatology in the upper troposphere over Reunion Island suggest multiple stratospheric intrusions. Biomass burning activities were not detected on satellite images over countries bordering the South-West Indian Ocean the previous weeks, and no significant electric activity (i.e., lightning strokes [*Jacobson et al.*, 2006]) was detected on the World Wide Lightning Location Network data. The ozone anomalies are then very likely not associated with an on-site production in the troposphere by chemical processes. Explanations for their origins have to be searched assuming irreversible stratosphere-troposphere transport. In the following sections, further investigations are presented to interpret in more details the vertical structure of these peaks, to document their multiple stratospheric origins, and to assess their corresponding residence times in the upper troposphere.

3.2. Synoptic Setting

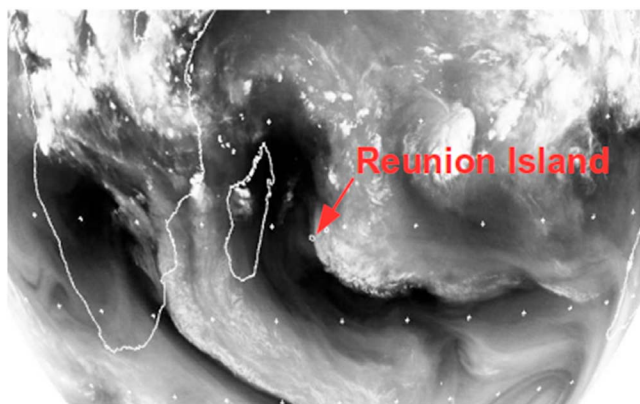


Figure 2. Meteosat image in the water vapor channel on 4 April 2013 at 1800 UTC.

Figure 3 shows the water vapor, the ozone mixing ratio, and the potential vorticity at 350 K from ECMWF ERA-Interim re-analysis on 4 April at 1800 UTC. The water vapor mixing ratio at 350 K (Figure 3a) is in agreement with the Meteosat image (Figure 2), showing two synoptic-scale dry air filaments at the longitudes of Reunion Island and over the south-eastern coast of Africa. As shown by the ERA-Interim analysis, these filaments are rich in ozone (Figure 3b) and are associated with PV values (lower than or equal to

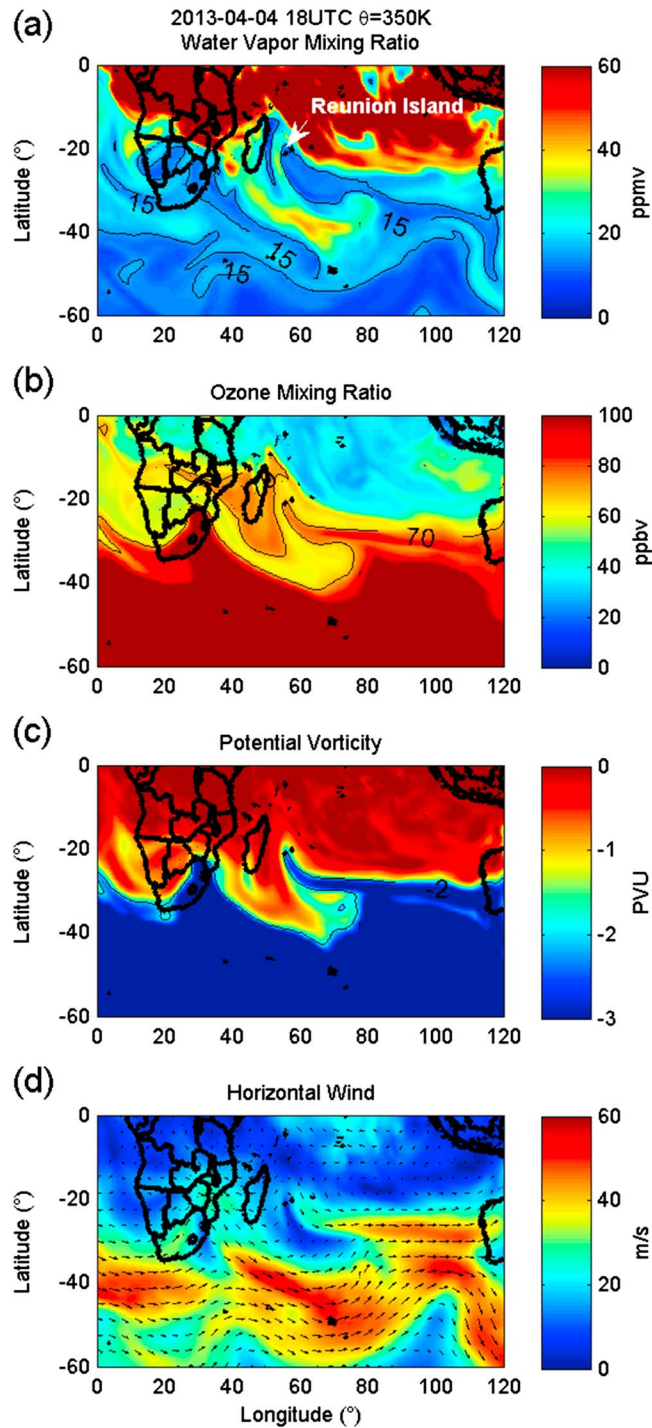


Figure 3. ECMWF ERA-Interim re-analysis on 4 April 2013 at 1800 UTC for (a) water vapor mixing ratio (in ppmv), (b) ozone mixing ratio (in ppbv), (c) potential vorticity (in PVU), and (d) wind speed (m s^{-1}) at 350 K. The black lines represent the 15 ppmv water vapor mixing ratio, the 70 ppbv ozone mixing ratio, and the -2 PVU potential vorticity contours in Figures 3a–3c, respectively.

-2 PVU) typical of the stratosphere (Figure 3c). The synoptic setting then describes a regime of RWB with meridional intrusions of dry and rich-ozone equatorward air masses, and inversely. It involves the dynamics of two upper level tropospheric jets (Figure 3d): the polar jet stream nearby and south of 40°S , and the subtropical jet stream mostly present at 250 hPa at lower latitudes.

Meridional vertical cross sections of water vapor and ozone mixing ratios, and potential vorticity from ECMWF ERA-Interim re-analysis on 4 April at 1800 UTC, are displayed on Figure 4. The zonal cross sections are quite symmetrical to the meridional ones. Over Reunion Island (position represented by a white segment in Figure 4), the RWB involves a strong tropopause break. The vertical structure of the water vapor mixing ratio field is the one of the three tracers that shows the least of vertical fine-scale structures and evidence of intrusions. Ozone and PV fields are strongly correlated. By contrast to water vapor, the latter fields clearly show that stratospheric intrusion processes are present down to 400–500 hPa.

To summarize, a complex synoptic setting associated with the dynamics of the subtropical and polar jet streams has to be considered over a time period of a few days to take into account the time scale of stratosphere-troposphere transport. While reproducing well a RWB event and the large-scale structures of the tropopause, the ECMWF analyses do not provide the detailed structures shown on the ozone lidar profile. With regard to the vertical layering, only one peak of ozone and PV can be inferred from vertical cross-

sections (Figure 4), whereas ozone lidar profiles show three peaks. To ensure that the misrepresentation did not come from the vertical resolution chosen (37 pressure levels), an ozone mixing ratio cross section based on the whole ERA-Interim model levels has been plotted (not shown). With the full vertical resolution

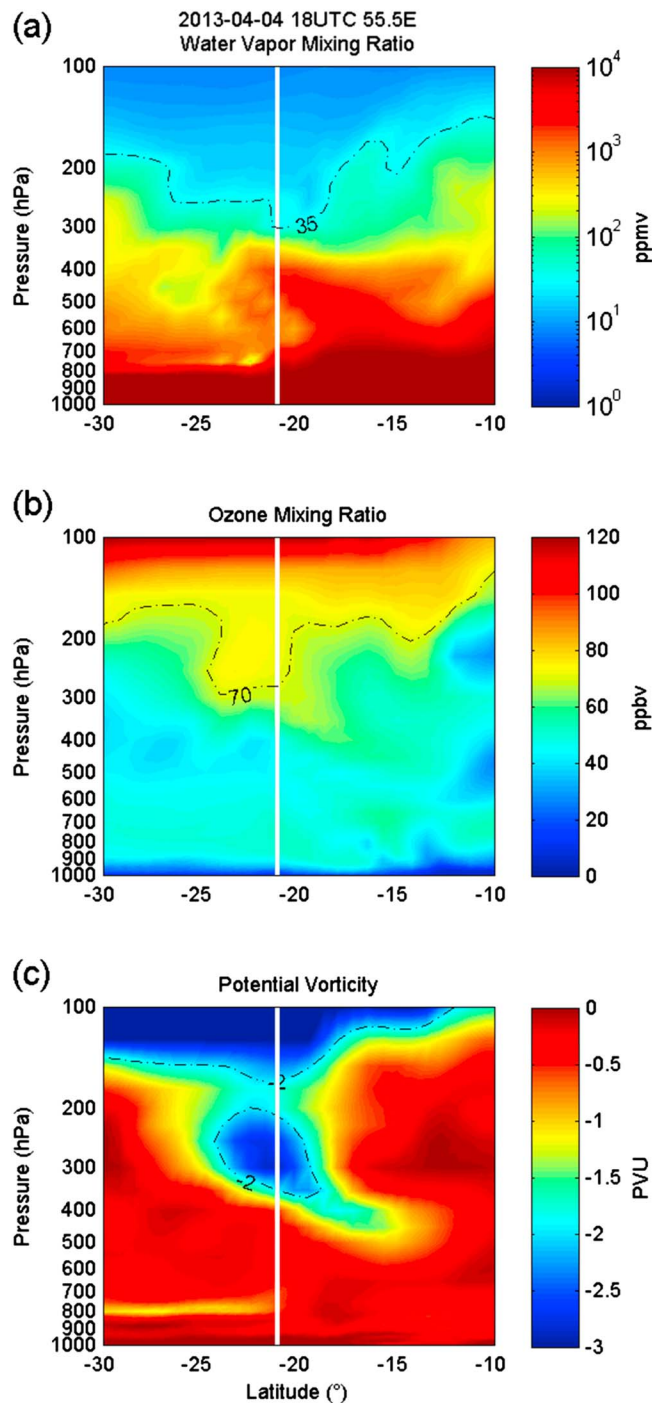


Figure 4. Meridional vertical cross sections from ECMWF ERA-Interim re-analysis on 4 April 2013 at 1800 UTC for (a) water vapor mixing ratio (ppmv, with a logarithmic color scale), (b) ozone mixing ratio (ppbv), and (c) potential vorticity (PVU). The white vertical lines indicate the position of Reunion Island. The black lines represent the 35 ppmv water vapor mixing ratio, the 70 ppbv ozone mixing ratio, and the -2 PVU potential vorticity contours in Figures 4a–4c.

approximately 40 ppmv at the top of the profiles. The magnitudes of ozone and water vapor mixing ratios for peak nos. 2 and 3 (in excess of 90 ppbv for ozone and dryer than 30 ppmv for water vapor) suggest air originating from the stratosphere for both peaks. The radiosounding profile closest in time to the ozone lidar profile

of the model, no more significant structures or peaks appeared. ECMWF ozone fields in the upper troposphere are not always robust in some synoptic situations [Dethof and Hólm, 2004]. The problem has not yet been solved in the re-analysis, and it is recognized that this issue should be considered for the next re-analysis project [Dragani, 2011; Dragani and Dee, 2008]. Few studies [e.g., Bithell et al., 2000; D'Aulerio et al., 2005; Gouget, 2000] highlighted that global model analyses may not represent vertically thin structures associated with STE.

3.3. Fine-Scale Vertical Layering

Getting back to observations in vertical profiles (Figure 1), a multispecies analysis is now attempted to better interpret the stratospheric origin of the layers. One ozone lidar profile was performed per night during the campaign supported by one or several water vapor lidar and radiosounding profiles (Table 2).

With regard to the vertical profiles available on 2 April, there is none anticorrelation between water vapor and ozone suggesting a recent stratospheric origin of the ozone peak (peak 0) observed at 450 hPa (Figure 1a). For that kind of low-altitude ozone peak, Lagrangian techniques and/or mesoscale numerical simulations using a meteorological model with stratospheric tracers are necessary to go further to reproduce the vertical layering of the case study.

On 4 April, the ozone peak no. 1, that is the lowest in altitude, presents the narrowest vertical width of the three ozone peaks and is linked to the highest water vapor mixing ratio. Water vapor mixing ratio ranges from a few hundreds of ppmv in the lowest altitudes to approxi-

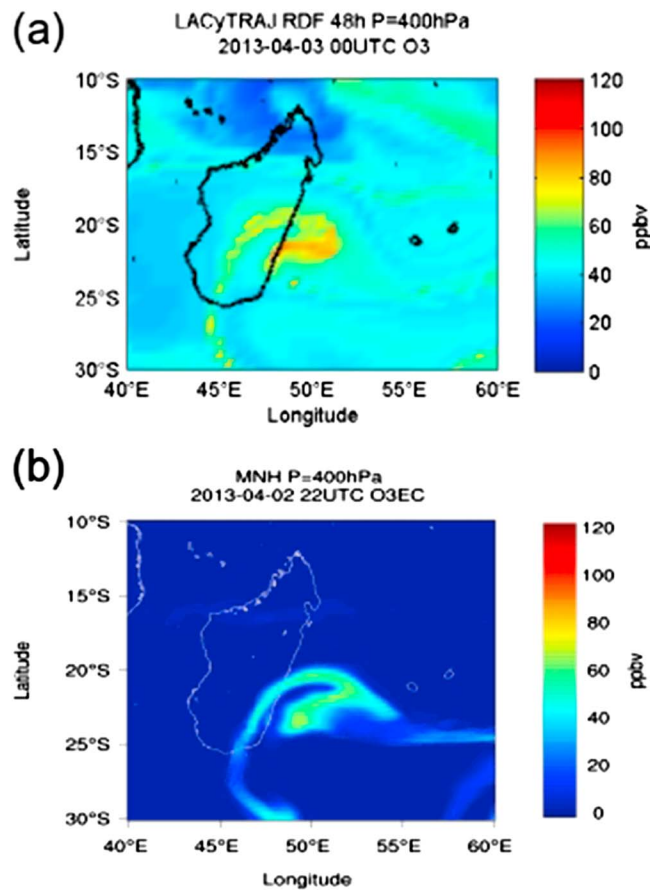


Figure 5. (a) 400 hPa ozone mixing ratio (ppbv) on 3 April at 0000 UTC with the LACYTRAJ-RDF method (48-hours backward advection using ECMWF ERA-Interim re-analyses). (b) 400 hPa stratospheric tracer mixing ratio (ppbv) on 2 April 2013 at 2200 UTC from the Meso-NH simulation. The stratospheric tracer is initialized at the beginning of a dedicated simulation on 1 April 0000 UTC.

planning a highly spatiotemporal variable field [Vogelmann *et al.*, 2015; Wang *et al.*, 2010] in the complex fine-scale structure of the upper level trough and its associated frontal zones. It may also come from the different metrologies, such as sensitivity, response times, and vertical resolution for the radiosonde sensors, and time integration period, calibration factor, and vertical resolution for the lidar. It should also be pointed out that the lidar setup and its configuration were not optimal because it was one of the first measurements of the campaign. The time period for integration of the lidar signal was generally short (about 30 min), while more recent campaigns have shown that a minimum 40 min integration time is required for upper tropospheric measurements with standard errors (results in progress, not shown). The calibration factor was difficult to determine during this campaign and especially this night during which different instrumental configurations have been tested, tests which could impact this factor. Nevertheless, the reliability of both types of measurements is set and useful information have been pointed out regarding the stratospheric origin of ozone peaks observed on 4 April 2013.

3.4. Lagrangian History and Mesoscale Modeling

With regard to ozone peak 0 observed on 2 April (Figure 1a), results for the RDF Lagrangian model and for the Meso-NH model are shown on Figure 5. The model simulations are a run of Meso-NH initialized on 1 April at 0000 UTC and LACYTRAJ runs initialized on the domain: 250 to 450 hPa, 10°S–30°S and 45°E–70°E on 2 and 3 April. Although the techniques used are completely different, the ozone fields of stratospheric origin that are reproduced strongly resemble each other, both in the structure and in the intensity. It draws a filament of air originating from the stratosphere which has been transported down to the middle troposphere (400 hPa) above

(1516 UTC and 1610 UTC, respectively) shows an extremely dry layer centered at 10 km altitude in strong anticorrelation with peak no. 2, which reinforces its stratospheric-origin hypothesis. The next radiosoundings show that the extremely dry layer has widened and taken aloft at about 10.5 km altitude (1956 UTC) and is no longer present later on (2212 UTC). However, water vapor lidar profiles from 1635 UTC to 2210 UTC do not show evidence of such an extremely dry layer even if a very dry upper troposphere (water vapor mixing ratio < 100 ppmv) is remotely sensed. Water vapor mixing ratio differences observed between radiosondes and lidar measurements may have several explanations. The measurement technique of the lidar could explain the difficulty of observing the strict anticorrelation of the ozone peak no. 2. Since the structure rose of about 800 m in 7 h and moved in longitude, the gradient may have been smoothed by the integration that would make it difficult to see on the lidar profiles. Thus, differences may come from the noncoincidence in time and in space for two instruments sam-

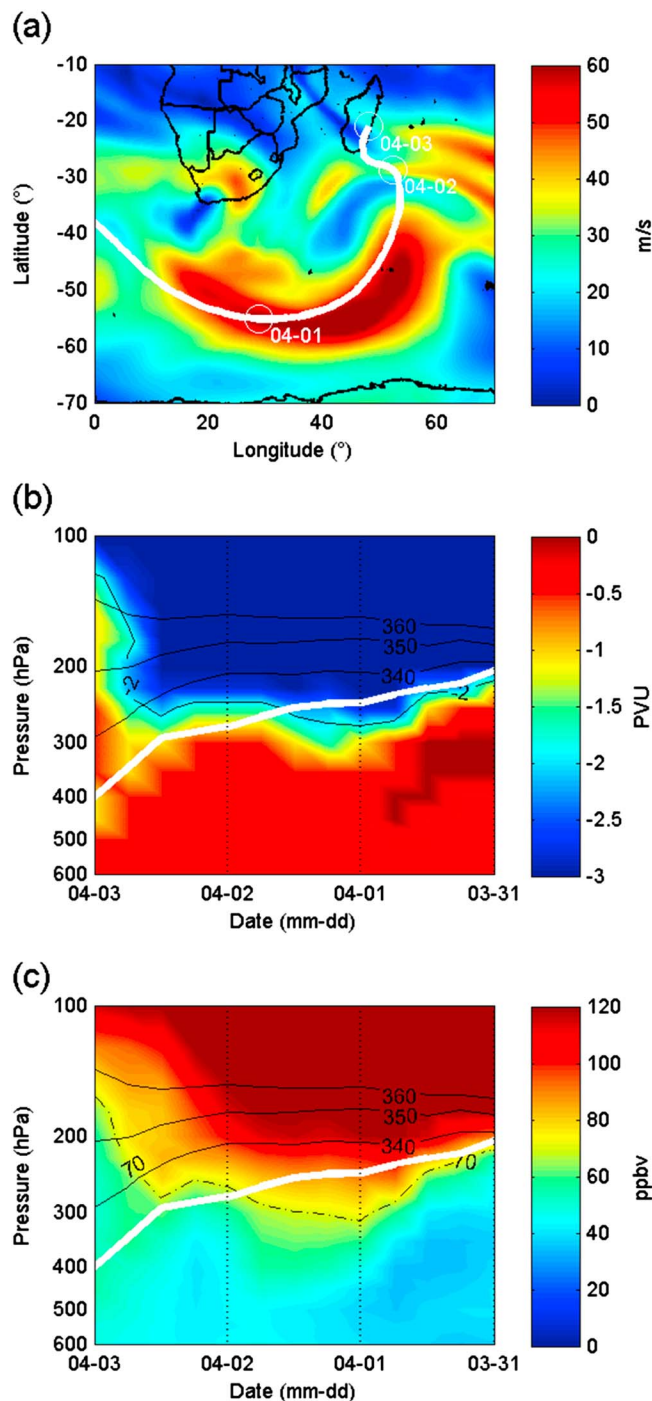


Figure 6. (a) 200 hPa wind speed (m s^{-1}) on 1 April at 1200 UTC from ECMWF ERA-Interim re-analysis. The white line is the LACYTRAJ back trajectory initialized on a grid point located at 21°S , 48°E , and 400 hPa on 3 April 2013 at 0000 UTC. The circles indicate the geographical location of the particle for each day (mm-dd) at 0000 UTC. Time series of vertical profiles of (b) potential vorticity (PVU) and (c) ozone mixing ratio (ppbv) from ECMWF ERA-Interim re-analysis along the back trajectory shown with a white line in Figure 6a. The black solid and dashed lines in Figures 6b and 6c represent the 340, 350, and 360 K isentropic levels, and the -2 PVU isocontour, respectively.

the trade wind inversion. The exchange with the stratosphere is irreversible as the filament is no longer associated with the upper level dynamics and is then destined to be mixed in the troposphere. The simulations show that the stratospheric intrusion displayed on Figure 5 moves later on north of Reunion Island and does not reach the island. The filament of stratospheric origin has not been advected up to the longitude of Reunion Island. The distances associated with the stratospheric intrusion process are synoptic-scale; it is the same order of magnitude than the distances traveled by air particles during their tropospheric residence times; i.e., a few thousands of kilometers. Therefore, an acceptable uncertainty on the location of the filament would be a few hundreds of kilometers. The shortest distance between the Maïdo Observatory and the 60 ppbv ozone isocontour in the southwest direction is less than 300 km with both methods, which is an acceptable uncertainty with regard to the distances associated with the stratospheric intrusion process. The back trajectory of the air parcel initialized in the filament shows that the crossing of the tropopause of these air masses is strongly associated with the polar jet stream (Figures 6a and 6b). This is consistent with the low altitude reached by the intrusion (compared to the altitudes of the intrusions associated with the higher subtropical jet stream). Records of PV and ozone along the back trajectory (Figures 6b and 6c, respectively) show that the residence time of the air parcel in the troposphere after leaving the stratosphere is of about 36 h and that the ozone mixing ratio of air parcels when in the lower stratosphere is of about 80–90 ppbv. The last two estimations are reconcilable with the action of tropospheric mixing processes to diminish the ozone mixing

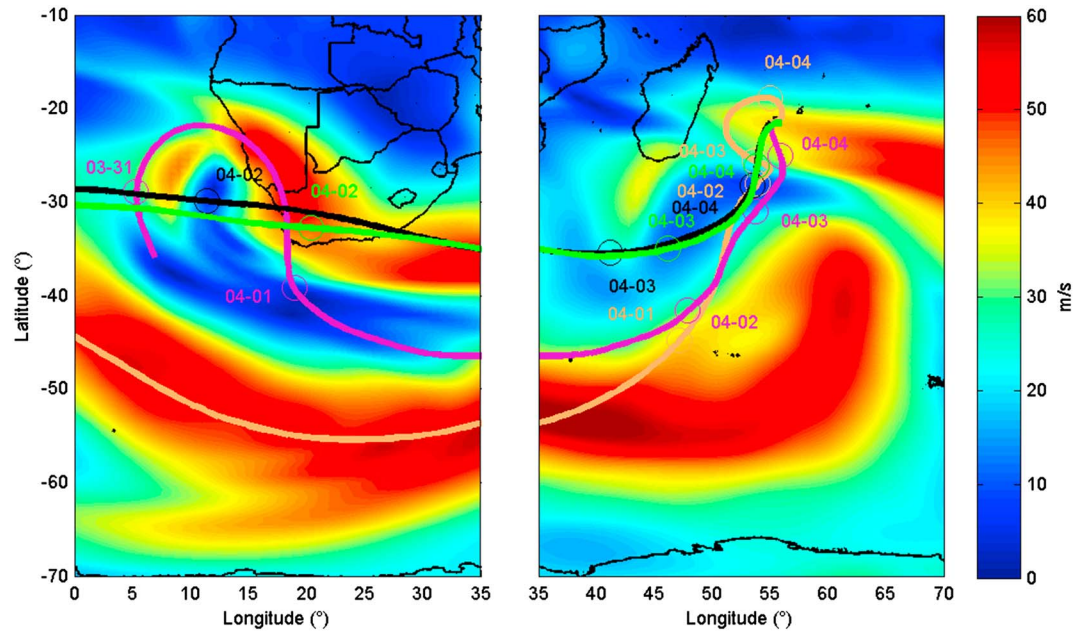


Figure 7. Wind speed (m s^{-1}) at 350 K on (left) 31 March at 1200 UTC and on (right) 2 April at 0000 UTC from ECMWF ERA-Interim re-analysis. The orange, violet, black, and green lines are LACYTRAJ 5-day back trajectories initialized on 4 April 2013 at 1800 UTC on the grid point ($21.5^{\circ}\text{S}, 55^{\circ}\text{E}$) at 350 hPa, 280 hPa, and 200 hPa, and on the grid point ($21.5^{\circ}\text{S}, 56^{\circ}\text{E}$) at 200 hPa, respectively. The circles indicate the geographical location of the particles for each day (mm-dd) at 0000 UTC.

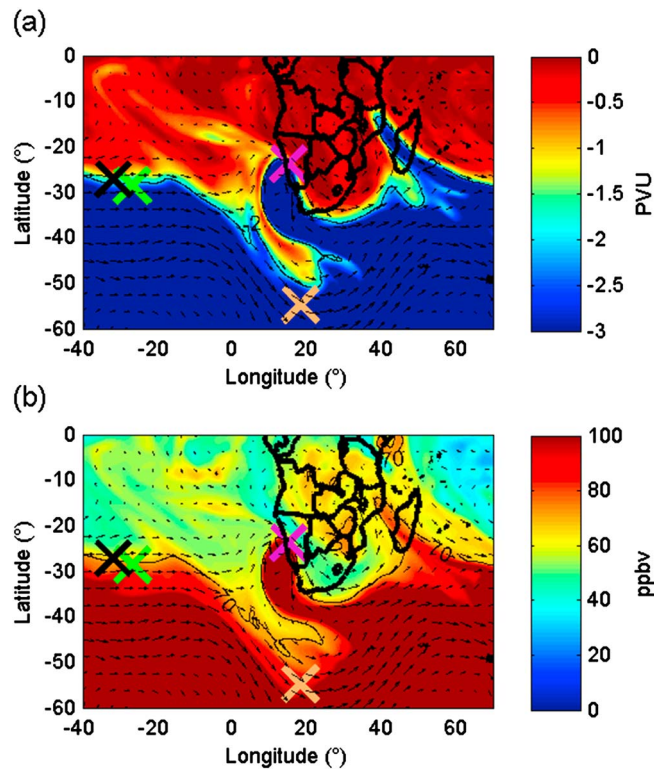


Figure 8. (a) Potential vorticity (PVU) and (b) ozone mixing ratio (ppbv) at 350 K on 31 March at 1200 UTC from ECMWF ERA-Interim re-analysis. The crosses represent the position of the particles along the backward trajectories in Figure 7 on 31 March 2013 at 1200 UTC with the same color code as in Figure 7.

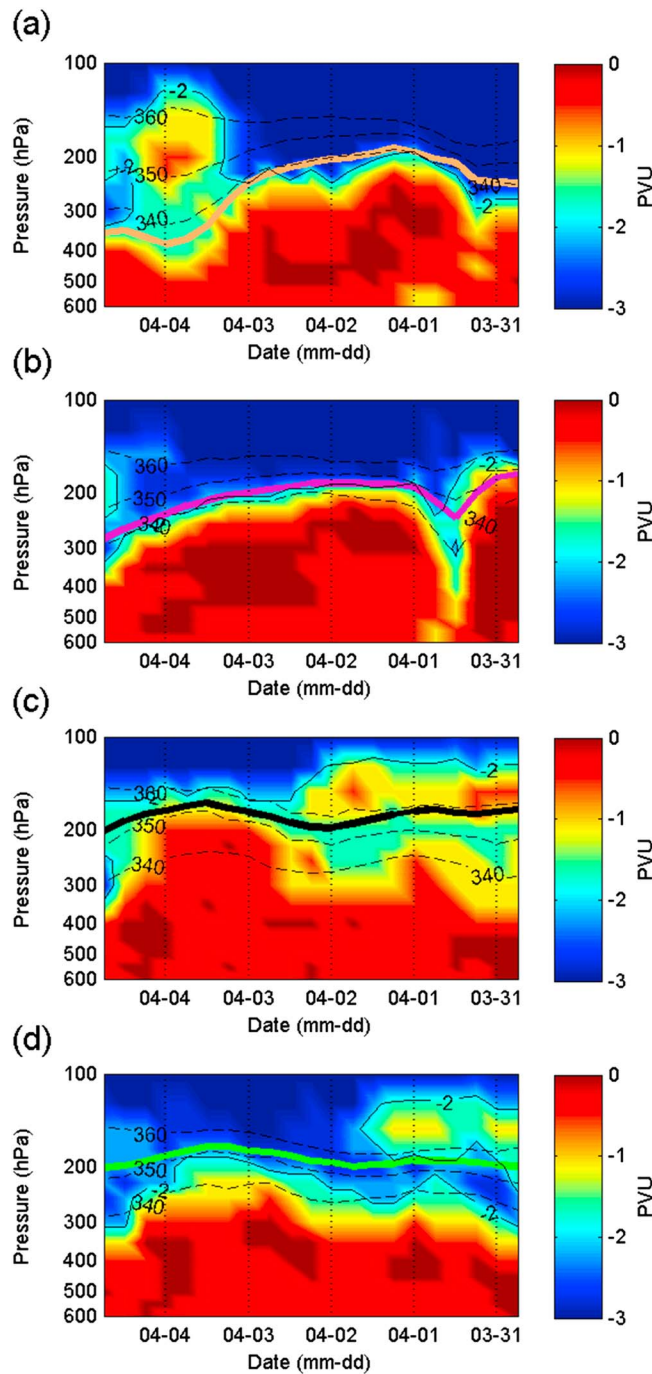


Figure 9. Time series of vertical profiles of potential vorticity (PVU) from ECMWF ERA-Interim re-analysis along the back trajectories shown in Figure 7. The black lines represent the 340, 350, and 360 K isentropic levels (dotted) and the -2 PVU contour (solid).

assess as the air particles constantly have followed the edge of the tropopause break (Figure 8b). Brought in a Rossby wave, the particles met on the path over South Africa cloud convection as it can be seen in satellite images and in ECMWF convective precipitations fields (not shown). This could have induced some moistening of the air masses. Nevertheless, the associated lidar water vapor observations confirm the recent stratospheric origins (dryness and ozone anticorrelation).

ratio down to 60 ppbv in Reunion Island. Although not being strictly reproduced by the models, this observation of the first ozone peak at the Maïdo Observatory was worth to be documented.

Back to the observations on 4 April 2013, we now trace the history of atmospheric particles which are representative of the two ozone peak nos. 1 and 2 (Figures 7–10). Peak no. 1 is associated with particles involved in the polar jet stream dynamics south of latitude 40°S (Figure 7, left, orange back trajectory). While it is clear that peak no. 2 is associated with particles involved in the subtropical jet stream dynamics north of latitude 40°S (Figure 7, left, violet back trajectory). At the synoptic scale, particles associated with peak nos. 1 and 2 are following the polar edges of the tropopause break as drawn by the isentropic gradients of PV and ozone on Figure 8. Particles associated with peak no. 1 stayed in the polar stratospheric reservoir up to longitude 50°E , while particles associated with peak no. 2 already had incursions in the subtropics at longitude 10°E . Particles associated with peak no. 1 stayed below the 340 K isentropic surface (Figure 9). Their residence time into the troposphere is about 36 h (Figure 9a). Lidar water vapor observations of this peak show that the anticorrelation with ozone is no more observed (Figure 1b), which indicates that mixing processes with more humid lower tropospheric air masses are at work. It makes clear that the stratosphere-troposphere transport for the latter particles is irreversible. With regard to peak no. 2, particles stayed above the 340 K isentropic surface (Figure 9b). Residence time into the troposphere for air particles associated with peak no. 2 is difficult to

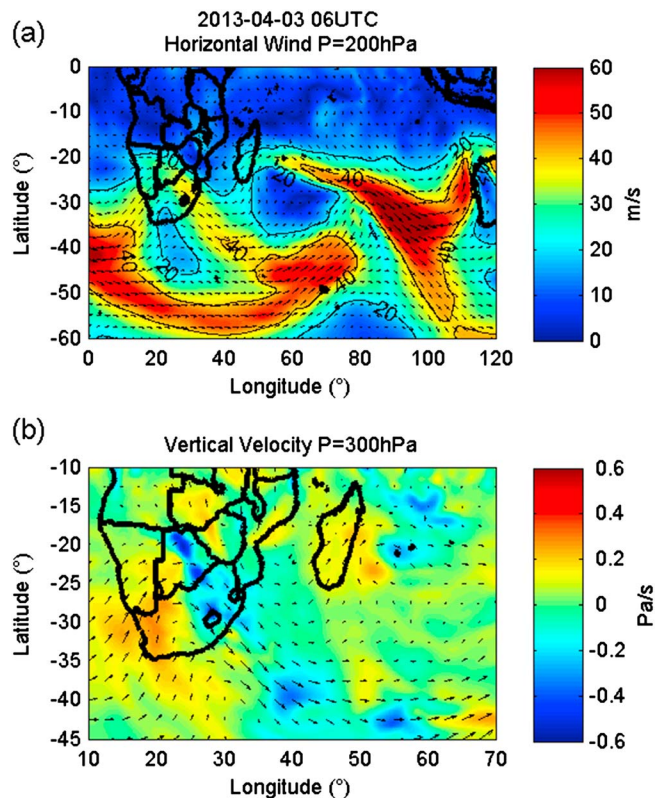


Figure 10. (a) Horizontal wind speed (m/s) at 200 hPa and (b) vertical velocity (Pa/s) at 300 hPa (zoom) on 3 April at 0600 UTC from ECMWF ERA-Interim re-analysis.

As presented above, particles associated with peak nos. 1 and 2 were guided as a first step (west of 30°E and before 2 April) by the dynamics of the polar jet stream and by the dynamics of the subtropical jet stream, respectively. It is now shown that in the final phase (east of 40°E and starting from 3 April) particles associated with both peaks are guided only by the dynamics of the subtropical jet stream. Figure 10a shows that these particles are moving toward the entrance region of the subtropical jet between Madagascar and Reunion Island. Through the combined effects of acceleration and curvature in the entrance region of the subtropical jet [Keyser and Shapiro, 1986], a dipole of vertical velocity (Figure 10b) has set up with descent east of Madagascar and ascent over Reunion Island. Entering the descent pole, both particles associated with peak nos. 1 and 2 subside along the upper level frontal zones beneath the subtropical jet (Figures 9c and 9d).

The intrusion of particles associated with peak no. 2 stays on the polar side of the subtropical jet (Figure 7, right). Processes are approximately adiabatic because potential vorticity and potential temperature are conserved to a certain extent from 3 to 4 April (Figure 9c). Mixing effects have a negligible impact on this intrusion which is consistent with the ozone and water vapor mixing ratios anticorrelation observed between lidar and radiosonde data (Figure 1). During the intrusion associated with peak no. 1, particles pass on the equator side the subtropical jet axis (Figure 7, right). The time series of potential vorticity profiles along the trajectory (Figure 9d) clearly show high-altitude subtropical tropopauses above the particles when following a cyclonic circulation back to Reunion Island (Figure 7, right). Processes during this deeper intrusion into the subtropical upper troposphere are not adiabatic because particles loose potential vorticity and shift down to lower isentropic surfaces from 3 to 4 April (Figure 9d). Effects of diabatic mixing associated with clear-air turbulence in the upper level frontal zone are responsible of the decorrelation that occurs between stratospheric-origin ozone and more humid layers below 9 km altitude (Figure 1).

With regard to peak no. 3, it was not possible to demonstrated that it is a stratospheric intrusions associated with the dynamics of the subtropical jet stream above 350 K. Rather than a stratospheric intrusion, peak no. 3 is interpreted here as a brief period of scanning of the lidar beam at 11–13 km asl across the stratospheric reservoir. It occurs at the tropopause break where the tropopause is structured as a quasi-vertical wall following the edges of the upper level trough associated with the Rossby wave. This is achieved by the movement of the tropopause break during the time integration period needed to build the ozone vertical profile with the lidar (>1 h). Back trajectories of two air particles situated at the same latitude (21.5°S) but with a small shift in longitude (55°E and 56°E; Figures 9c and 9d, respectively) across the tropopause break (see Figure 2) show almost identical pathways (Figure 7), while PV records (Figure 9) clearly indicate that air particles stay within their own tropospheric or stratospheric reservoir.

Figure 11 shows meridional cross sections from RDF-LACYTRAJ and Meso-NH equivalent to those derived from ECMWF analysis (see Figure 4). It is important to remember that the ozone fields represented by the

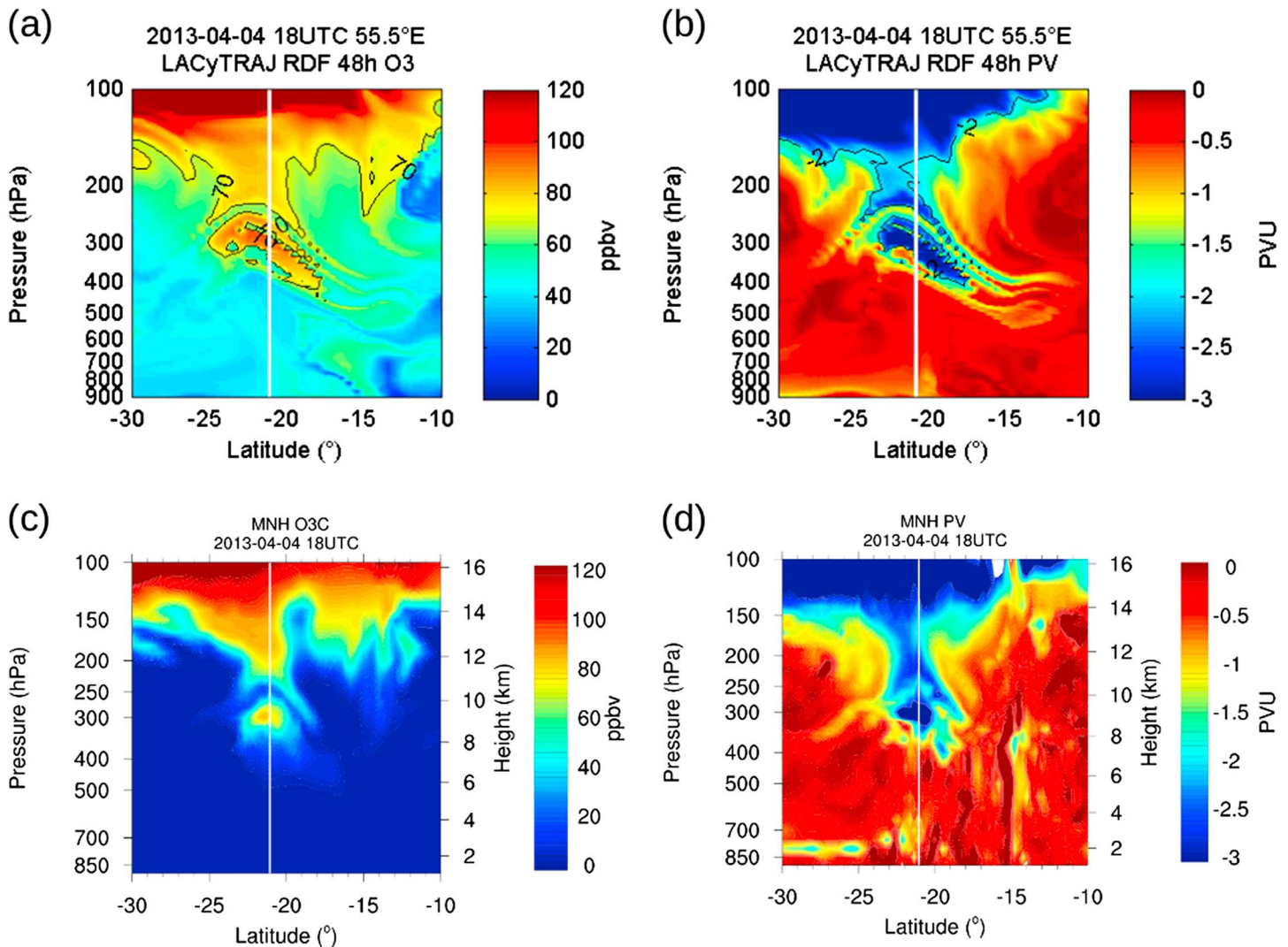


Figure 11. Meridional vertical cross sections at 55.5°E on 4 April 2013 at 1800 UTC. (a) Ozone mixing ratio and (b) potential vorticity with LACyTRAJ-RDF method (48 h backward advection using ECMWF ERA-Interim re-analyses). (c) Stratospheric ozone mixing ratio tracer and (d) potential vorticity from Meso-NH. The white lines indicate the position of Reunion Island. The black dashed lines indicate the 70 ppbv and -2 PVU isocontours for ozone mixing ratio and potential vorticity, respectively (Figures 11a and 11b).

two models are not equivalent: the RDF-LACyTRAJ cross section represents ozone from 2 day backward trajectories initialized over the whole domain (Figure 11a), whereas Meso-NH runs forward in time a passive stratospheric ozone tracer (with the threshold of 70 ppbv) during 2 days (Figure 11c). On 4 April, a maximum of ozone, around 350 hPa and higher than 80 ppbv, is represented by a 2 day run (Figures 11a and 11c). A column of ozone linked to the stratospheric reservoir can also be seen in the troposphere up to 250 hPa (Figures 11a and 11c). LACyTRAJ and Meso-NH representations of the intrusion are essentially very similar (Figures 11b and 11d). Even if the variables representing the ozone come from different methodologies, the values for the tracer simulated by Meso-NH on 4 April are consistent with the observations and the RDF calculations. Even if the chemistry is not activated, Meso-NH represents in details the vertical and horizontal distributions regarding ozone and PV, in agreement with the observations and the Lagrangian reconstruction. For such a mesoscale Eulerian modeling, the vertical resolution is a key factor to simulate such large-scale processes while retrieving precisely its vertical and horizontal fine-scale structures.

As for the case of 2 April (Figure 5), ozone and PV fields produced by the two numerical approaches are again very similar. With regard to ozone peak nos. 1 and 2 on 4 April, the modeled ozone and PV fields confirm how the peaks are a part of tropopause folds associated with the polar and subtropical jet streams, respectively.

Ozone mixing ratios within the modeled stratospheric intrusions match well to lidar observations (80–90 ppbv), despite inherent simplifications in numerical simulations, like turbulent mixing processes which are missing in the RDF technique, and ozone tropospheric photochemistry which is missing in both techniques. The results show that the two techniques used herein, the Lagrangian RDF technique and the advection of a stratospheric tracer with the Meso-NH Eulerian model, are suitable to investigate stratosphere-troposphere transport processes.

4. Conclusion

In this paper, we have analyzed a situation of multiple stratospheric intrusions associated with the dynamics of the polar and subtropical jet streams over the south-west Indian Ocean. The combined use of in situ and remote sensing observations, synoptic analyses, and numerical modeling has allowed to (1) detect and validate assumptions of stratospheric intrusions and (2) trace back the history of the intrusions. The modeling results show that both Lagrangian and Eulerian models can be used to diagnose and interpret STE processes. The Meso-NH model run with a high vertical resolution (150 m for vertical grid-spacing) well reproduces the complex situation of multiple stratospheric intrusions.

Results indicate that the dynamics of the polar and of the subtropical jet streams are each one responsible for the stratospheric-origin ozone intrusions in the troposphere, at 6.8 and 8.2 km altitude for the polar jet stream, and at 9.9 km altitude for the subtropical jet stream. The significant tropospheric residence times and distances in latitude and altitude between these three intrusions and the stratospheric reservoir indicate that a part of the stratosphere-troposphere transport is irreversible. It remains to be seen whether or not these multiple stratospheric intrusions refer to the possible existence of a regional specificity. Furthermore, results anecdotally show that the highest ozone peak observed under the tropopause is not a signature of stratosphere-troposphere transport. It is a result of the combined effect of the time integration period needed for the ozone lidar measurements and of the position of the lidar beneath strong and moving ozone horizontal gradients along the edge of the tropopause break. The modeling results indicate that providing that a suitable vertical resolution is chosen in mesoscale modeling exercises with a regular horizontal resolution (about 20 km), complex intrusion processes might be well represented, thanks to the dynamics of the model and the parametrization schemes controlling the mixing. No chemistry was needed to be activated in Meso-NH to simulate the event in agreement with the observations. The results also show that progress has been made in the representation of the stratospheric ozone in global analyses of Global and regional Earth-system Monitoring using Space and in situ data Atmospheric Service. The use of this field to initialize passive stratospheric tracer in the mesoscale modeling of the STE has been efficient to reconstitute the fine-scale layering of the ozone distribution observed above Reunion Island for the case study.

As a follow-up to this work, it would be possible to run budget calculation in Meso-NH to quantify the irreversible part of the stratosphere-to-troposphere transport. The study has also highlighted the difficulty in using water vapor as a tracer of stratosphere-troposphere transport in the subtropics. Indeed, the complex vertical layering shown by the lidar and sonde measurements in the extreme dry environment of the upper troposphere is challenging both observation and modeling tools for producing high vertical resolution. With high-resolution water vapor and ozone profiles coming soon from more efficient devices (sondes and lidars), a new focus of research on the lifetime and the impact of stratospheric intrusions in the troposphere could be initiated in Reunion Island and push forward STE studies in the subtropics. The lidar technique and the Lagrangian and mesoscale modeling approaches represent interesting tools to characterize such events regarding the air parcel origins, the irreversibility of transport, and mixing processes. The strength of the Maïdo Observatory is that the facility offers a set of several collocated lidars that are committed to deliver, twice a week on a routine basis following the recommendations of NDACC, high vertical resolution observations of ozone and water vapor mixing ratio profiles. It heightens the role of the Maïdo high-altitude station facility in delivering routine and high-quality atmospheric measurements for process studies and for long-term surveys in the subtropics.

Our modeling results confirm that the vertical resolution of global chemistry transport models needs to be improved in order to (i) resolve the multiplicity of the STE processes and (ii) better take account of the irreversible transport term associated to STE for the tropospheric ozone budget. Such an event is characteristic

of irreversible stratosphere-troposphere transport. These events, taken as a whole, may impact the tropospheric ozone budget in subtropical areas. This issue merits further study.

Acknowledgments

The Meteosat image is credited to NERC Satellite Receiving Station (<http://www.sat.dundee.ac.uk/>), Dundee University, Scotland. ECMWF ERA-Interim and CAMS Near-real time data used in this study have been obtained from the ECMWF data server (<http://apps.ecmwf.int/datasets/>). Thanks to CNRS (Centre National de la Recherche Scientifique) and the University of Reunion Island for funding the PhD of H. Vèrèmes and the MALICCA campaigns, the working groups ROSEA and GRUAN France, all people involved during MALICCA-1: Y. Courcoux, A. Hauchecorne, T. Gaudo, F. Gabarrot, J.-M. Metzger, and J. Porteneuve, and all the lidar/radiosonde operators. Also, the authors thank J. Brioude and S. Evan for their highlights on the Lagrangian modeling, G. Clain from MeteoModem for her highlights on the M10 profiles, and F. Gabarrot for his work on LACYTRAJ. This research was supported by the LEFE INSU-CNRS French Program under the project VAPEURDO. The work was granted access to the HPC resources of CINES under the allocation 2014-c2014017260 and 2015-c2015017260 made by GENCI. Some computations have been performed on the supercomputers facilities of Météo-France and on the supercomputer facilities of the University of Reunion Island.

References

- Ancellet, G., M. Beekmann, and A. Papayannis (1994), Impact of a cutoff low's development on downward transport of ozone in the free troposphere, *J. Geophys. Res.*, *99*, 3451–3468, doi:10.1029/93JD02551.
- Appenzeller, C., and H. C. Davies (1992), Structure of stratospheric intrusions into the troposphere, *Nature*, *358*(6387), 570–572.
- Appenzeller, C., H. C. Davies, and W. A. Norton (1996), Fragmentation of stratospheric intrusions, *J. Geophys. Res.*, *101*(D1), 1435–1456, doi:10.1029/95JD02674.
- Baray, J.-L., G. Ancellet, F. G. Taupin, M. Bessafi, S. Baldy, and P. Keckhut (1998), Subtropical tropopause break as a possible stratospheric source of ozone in the tropical troposphere, *J. Atmos. Sol. Terr. Phys.*, *60*(1), 27–36.
- Baray, J.-L., J. Leveau, J. Porteneuve, G. Ancellet, P. Keckhut, F. Posny, and S. Baldy (1999), Description and evaluation of a tropospheric ozone LIDAR implemented on an existing LIDAR in the southern subtropics, *Appl. Opt.*, *38*(33), 6808–6817.
- Baray, J.-L., V. Daniel, G. Ancellet, and B. Legras (2000), Planetary-scale tropopause folds in the southern subtropics, *Geophys. Res. Lett.*, *27*(3), 353–356, doi:10.1029/1999GL010788.
- Baray, J.-L., S. Baldy, R. D. Diab, and J. P. Cammas (2003), Dynamical study of a tropical cut-off low over South Africa, and its impact on tropospheric ozone, *Atmos. Environ.*, *37*(11), 1475–1488.
- Baray, J.-L., et al. (2006), An instrumented station for the survey of ozone and climate change in the southern tropics, *J. Environ. Monit.*, *8*(10), 1020–1028.
- Baray, J.-L., G. Clain, M. Plu, E. Feld, and P. Caroff (2010), Occurrence of monsoon depressions in the Southwest Indian Ocean: Synoptic descriptions and stratosphere to troposphere exchange investigations, *J. Geophys. Res.*, *115*, D17108, doi:10.1029/2009JD013390.
- Baray, J.-L., V. Duflot, F. Posny, J.-P. Cammas, A. M. Thompson, F. Gabarrot, J.-L. Bonne, and G. Zeng (2012), One year ozonesonde measurements at Kerguelen Island (49.2°S, 70.1°E): Influence of stratosphere-to-troposphere exchange and long-range transport of biomass burning plumes, *J. Geophys. Res.*, *117*, D06305, doi:10.1029/2011JD016717.
- Baray, J.-L., et al. (2013), Maïdo observatory: A new high-altitude station facility at Reunion Island (21°S, 55°E) for long-term atmospheric remote sensing and in-situ measurements, *Atmos. Meas. Tech.*, *6*, 2865–2877.
- Bechtold, P., E. Bazile, F. Guichard, P. Mascart, and E. Richard (2001), A mass-flux convection scheme for regional and global models, *Q. J. R. Meteorol. Soc.*, *127*(573), 869–886.
- Berrisford, P., D. Dee, P. Poli, R. Brugge, K. Fielding, M. Fuentes, P. Kallberg, S. Kobayashi, S. Uppala, and A. Simmons (2011), The ERA-Interim archive, version 2.0. ERA report series. 1. Technical Report. ECMWF, 23 pp.
- Bithell, M., G. Vaughan, and L. J. Gray (2000), Persistence of stratospheric ozone layers in the troposphere, *Atmos. Environ.*, *34*(16), 2563–2570.
- Bougeault, P., and P. Lacarrère (1989), Parameterization of orography-induced turbulence in a Mesobeta—Scale model, *Mon. Weather Rev.*, *117*(8), 1872–1890.
- Bourqui, M. S. (2006), Stratosphere-troposphere exchange from the Lagrangian perspective: A case study and method sensitivities, *Atmos. Chem. Phys.*, *6*(9), 2651–2670.
- Bourqui, M. S., et al. (2012), A new global real-time Lagrangian diagnostic system for stratosphere-troposphere exchange: Evaluation during a balloon sonde campaign in eastern Canada, *Atmos. Chem. Phys.*, *12*(5), 2661–2679.
- Cariolle, D., and M. Déqué (1986), Southern hemisphere medium-scale waves and total ozone disturbances in a spectral general circulation model, *J. Geophys. Res.*, *91*(D10), 10,825–10,846, doi:10.1029/JD091iD10p10825.
- Cariolle, D., and H. Teyssède (2007), A revised linear ozone photochemistry parameterization for use in transport and general circulation models: Multi-annual simulations, *Atmos. Chem. Phys.*, *7*(9), 2183–2196.
- Chaboureaud, J.-P., and P. Bechtold (2005), Statistical representation of clouds in a regional model and the impact on the diurnal cycle of convection during Tropical Convection, Cirrus and Nitrogen Oxides (TROCCINOX), *J. Geophys. Res.*, *110*, D17103, doi:10.1029/2004JD005645.
- Clain, G., J.-L. Baray, R. Delmas, P. Keckhut, and J.-P. Cammas (2010), A Lagrangian approach to analyse the tropospheric ozone climatology in the tropics: Climatology of stratosphere–troposphere exchange at Reunion Island, *Atmos. Environ.*, *44*(7), 968–975.
- Colette, A., G. Ancellet, and F. Borch (2005), Impact of vertical transport processes on the tropospheric ozone layering above Europe. Part I: Study of air mass origin using multivariate analysis, clustering and trajectories, *Atmos. Environ.*, *39*(29), 5409–5422.
- Collins, W. J., R. G. Derwent, B. Garnier, C. E. Johnson, M. G. Sanderson, and D. S. Stevenson (2003), Effect of stratosphere-troposphere exchange on the future tropospheric ozone trend, *J. Geophys. Res.*, *108*(D12), 8528, doi:10.1029/2002JD002617.
- Cristofanelli, P., et al. (2003), Stratosphere-to-troposphere transport: A model and method evaluation, *J. Geophys. Res.*, *108*(D12), 8525, doi:10.1029/2002JD002600.
- Cristofanelli, P., P. Bonasoni, L. Tositti, U. Bonafè, F. Calzolari, F. Evangelisti, S. Sandrini, and A. Stohl (2006), A 6-year analysis of stratospheric intrusions and their influence on ozone at Mt. Cimone (2165 m above sea level), *J. Geophys. Res.*, *111*, D03306, doi:10.1029/2005JD006553.
- D'Aulerio, P., F. Fierli, F. Congeduti, and G. Redaelli (2005), Analysis of water vapor LIDAR measurements during the MAP campaign: Evidence of sub-structures of stratospheric intrusions, *Atmos. Chem. Phys.*, *5*(5), 1301–1310.
- Danielsen, E. F. (1968), Stratospheric-tropospheric exchange based on radioactivity, ozone and potential vorticity, *J. Atmos. Sci.*, *25*(3), 502–518.
- Danielsen, E., R. Bleck, J. Shedlovsky, A. Wartburg, P. Haagenson, and W. Pollock (1970), Observed distribution of radioactivity, ozone, and potential vorticity associated with tropopause folding, *J. Geophys. Res.*, *75*(12), 2353–2361, doi:10.1029/JC075i012p02353.
- Das, S. S., S. Sijikumar, and K. N. Uma (2011), Further investigation on stratospheric air intrusion into the troposphere during the episode of tropical cyclone: Numerical simulation and MST radar observations, *Atmos. Res.*, *101*(4), 928–937.
- Dee, D. P., et al. (2011), The ERA-Interim reanalysis: Configuration and performance of the data assimilation system, *Q. J. R. Meteorol. Soc.*, *137*(656), 553–597.
- Dethof, A., and E. V. Hölm (2004), Ozone assimilation in the ERA-40 reanalysis project, *Q. J. R. Meteorol. Soc.*, *130*(603), 2851–2872.
- Dionisi, D., et al. (2015), Water vapor observations up to the lower stratosphere through the Raman lidar during the Maïdo Lidar Calibration Campaign, *Atmos. Meas. Tech.*, *8*, 1425–1445.
- Donnadille, J., J.-P. Cammas, P. Mascart, D. Lambert, and R. Gall (2001), FASTEX IOP 18: A very deep tropopause fold. I: Synoptic description and modelling, *Q. J. R. Meteorol. Soc.*, *127*, 2247–2268, doi:10.1002/qj.49712757703.
- Dragani, R. (2011), On the quality of the ERA-Interim ozone reanalyses: Comparisons with satellite data, *Q. J. R. Meteorol. Soc.*, *137*(658), 1312–1326.

- Dragani, R., and D. Dee (2008), Progress in ozone monitoring and assimilation, *ECMWF Newsl.*, 116, 35–42.
- Draxler, R. R., and G. D. Hess (1998), An overview of the HYSPLIT_4 modeling system of trajectories, dispersion, and deposition, *Aust. Meteorol. Mag.*, 47, 295–308.
- Ebel, A., H. Hass, H. J. Jakobs, M. Laube, M. Memmesheimer, A. Oberreuter, H. Geiss, and Y.-H. Kuo (1991), Simulation of ozone intrusion caused by a tropopause fold and cut-off low, *Atmos. Environ., Part A*, 25(10), 2131–2144.
- Flentje, H., A. Dörnbrack, G. Ehret, A. Fix, C. Kiemle, G. Poberaj, and M. Wirth (2005), Water vapor heterogeneity related to tropopause folds over the North Atlantic revealed by airborne water vapor differential absorption lidar, *J. Geophys. Res.*, 110, D03115, doi:10.1029/2004JD004957.
- Gouget, H. (2000), Case study of a tropopause fold and of subsequent mixing in the subtropics of the Southern Hemisphere, *Atmos. Environ.*, 34(16), 2653–2658.
- Hegglin, M. I., et al. (2004), Tracing troposphere-to-stratosphere transport above a mid-latitude deep convective system, *Atmos. Chem. Phys.*, 4, 741–756, doi:10.5194/acp-4-741-2004.
- Hess, P. G., and R. Zbinden (2013), Stratospheric impact on tropospheric ozone variability and trends: 1990–2009, *Atmos. Chem. Phys.*, 13(2), 649–674.
- Hoareau, C., P. Keckhut, J.-L. Baray, L. Robert, Y. Courcoux, J. Porteneuve, H. Vömel, and B. Morel (2012), A Raman lidar at La Reunion (20.8°S, 55.5°E) for monitoring water vapour and cirrus distributions in the subtropical upper troposphere: Preliminary analyses and description of a future system, *Atmos. Meas. Tech.*, 5(6), 1333–1348.
- Holton, J. R., P. H. Haynes, M. E. McIntyre, A. R. Douglass, R. B. Rood, and L. Pfister (1995), Stratosphere-troposphere exchange, *Rev. Geophys.*, 33(4), 403–439, doi:10.1029/95RG02097.
- Hoskins, B. J., M. E. McIntyre, and A. W. Robertson (1985), On the use and significance of isentropic potential vorticity maps, *Q. J. R. Meteorol. Soc.*, 111(470), 877–946.
- Inness, A., J. Flemming, M. Suttie, and L. Jones (2009), GEMS data assimilation system for chemically reactive gases ECMWF Technical Memorandum n°587.
- Jacobson, A. R., R. Holzworth, J. Harlin, R. Dowden, and E. Lay (2006), Performance assessment of the World Wide Lightning Location Network (WWLLN), using the Los Alamos Sferic Array (LASA) as ground truth, *J. Atmos. Oceanic Technol.*, 23(8), 1082–1092.
- Keckhut, P., et al. (2015), Introduction to the Maïdo Lidar Calibration Campaign dedicated to the validation of upper air meteorological parameters, *J. Appl. Remote Sens.*, 9(1094099), doi:10.1117/1.JRS.9.094099.
- Kentarchos, A. S., G. J. Roelofs, and J. Lelieveld (1999), Model study of a stratospheric intrusion event at lower midlatitudes associated with the development of a cutoff low, *J. Geophys. Res.*, 104(D1), 1717–1727, doi:10.1029/1998JD100051.
- Keyser, D., and M. A. Shapiro (1986), A review of the structure and dynamics of upper-level frontal zones, *Mon. Weather Rev.*, 114(2), 452–499.
- Kley, D. (1997), Tropospheric chemistry and transport, *Science*, 276(5315), 1043–1044.
- Kuang, S., M. J. Newchurch, J. Burris, L. Wang, K. Knupp, and G. Huang (2012), Stratosphere-to-troposphere transport revealed by ground-based lidar and ozonesonde at a midlatitude site, *J. Geophys. Res.*, 117, D18305, doi:10.1029/2012JD017695.
- Lafore, J. P., et al. (1998), The Meso-NH Atmospheric Simulation System. Part I: Adiabatic formulation and control simulations, *Ann. Geophys.*, 16(1), 90–109.
- Leblanc, T., et al. (2011), Measurements of Humidity in the Atmosphere and Validation Experiments (MOHAVE)-2009: Overview of campaign operations and results, *Atmos. Meas. Tech.*, 4(12), 2579–2605.
- Leblanc, T., R. J. Sica, J. A. E. van Gijzel, S. Godin-Beekman, A. Haefele, T. Trickl, G. Payen, and F. Gabarrot (2016), Proposed standardized definitions for vertical resolution and uncertainty in the NDACC lidar ozone and temperature algorithms—Part 1: Vertical resolution, *Atmos. Meas. Tech. Discuss.*, 9, 4029–4049, doi:10.5194/amt-9-4029-2016.
- Leclair De Bellevue, J., A. Réchou, J.-L. Baray, G. Ancellet, and R. D. Diab (2006), Signatures of stratosphere to troposphere, transport near deep convective events in the southern subtropics, *J. Geophys. Res.*, 111, D24107, doi:10.1029/2005JD006947.
- Leclair De Bellevue, J., J. L. Baray, S. Baldy, G. Ancellet, R. Diab, and F. Ravetta (2007), Simulations of stratospheric to tropospheric transport during the tropical cyclone Marlene event, *Atmos. Environ.*, 41(31), 6510–6526.
- Lesouëf, D., F. Gheusi, R. Delmas, and J. Escobar (2011), Numerical simulations of local circulations and pollution transport over Reunion Island, *Ann. Geophys.*, 29(1), 53–69.
- Liu, G., J. Liu, D. W. Tarasick, V. E. Fioletov, J. J. Jin, O. Moeini, X. Liu, C. E. Sioris, and M. Osman (2013), A global tropospheric ozone climatology from trajectory-mapped ozone soundings, *Atmos. Chem. Phys.*, 13, 10,659–10,675, doi:10.5194/acp-13-10659-2013.
- Lu, J., C. Deser, and T. Reichler (2009), Cause of the widening of the tropical belt since 1958, *Geophys. Res. Lett.*, 36, L03803, doi:10.1029/2008GL036076.
- Luo, J., W. Tian, Z. Pu, P. Zhang, L. Shang, M. Zhang, and J. Hu (2013), Characteristics of stratosphere-troposphere exchange during the Meiyu season, *J. Geophys. Res. Atmos.*, 118, 2058–2072, doi:10.1029/2012JD018124.
- Meloan, J., et al. (2003), Stratosphere-troposphere exchange: A model and method intercomparison, *J. Geophys. Res.*, 108(D12), 8526, doi:10.1029/2002JD002274.
- Mlawer, E. J., S. J. Taubman, P. D. Brown, M. J. Iacono, and S. A. Clough (1997), Radiative transfer for inhomogeneous atmospheres: RRTM, a validated correlated-k model for the longwave, *J. Geophys. Res.*, 102(D14), 16,663–16,682, doi:10.1029/97JD00237.
- Newell, R. E., V. Thouret, J. Y. N. Cho, P. Stoller, A. Marengo, and H. G. Smit (1999), Ubiquity of quasi-horizontal layers in the troposphere, *Nature*, 398(6725), 316–319.
- Pinty, J.-P., and P. Jabouille (1998), A mixed-phase cloud parameterization for use in mesoscale non-hydrostatic model: Simulations of a squall line and of orographic precipitations, in *Proc. Conf. of Cloud Physics*, pp. 217–220, Am. Meteorol. Soc., Everett, Wash.
- Pommereau, J. P., and F. Goutail (1988), O₃ and NO₂ ground-based measurements by visible spectrometry during Arctic winter and spring 1988, *Geophys. Res. Lett.*, 15(8), 891–894, doi:10.1029/GL015i008p00891.
- Postel, G. A., and M. H. Hitchman (1999), A climatology of Rossby wave breaking along the subtropical tropopause, *J. Atmos. Sci.*, 56(3), 359–373.
- Reed, R. J. (1955), A study of a characteristic type of upper-level frontogenesis, *J. Meteorol.*, 12(3), 226–237.
- Reed, R. J., and E. F. Danielsen (1958), Fronts in the vicinity of the tropopause, *Arch. Meteorol. Geophys. Bioklimatol. A.*, 11(1), 1–17.
- Roelofs, G.-J., and J. Lelieveld (2000), Tropospheric ozone simulation with a chemistry-general circulation model: Influence of higher hydrocarbon chemistry, *J. Geophys. Res.*, 105(D18), 22,697–22,712, doi:10.1029/2000JD900316.
- Schoeberl, M. R., and P. A. Newman (1995), A multiple-level trajectory analysis of vortex filaments, *J. Geophys. Res.*, 100, 25,801–25,815, doi:10.1029/95JD02414.
- Schwarzkopf, M. D., and V. Ramaswamy (1993), Radiative forcing due to ozone in the 1980s: Dependence on altitude of ozone change, *Geophys. Res. Lett.*, 20(3), 205–208, doi:10.1029/93GL00209.

- Scott, R. K., and J.-P. Cammas (2002), Wave breaking and mixing at the subtropical tropopause, *J. Atmos. Sci.*, *59*(15), 2347–2361.
- Scott, R. K., J.-P. Cammas, P. Mascart, and C. Stolle (2001), Stratospheric filamentation into the upper tropical troposphere, *J. Geophys. Res.*, *106*(D11), 11, 835–11,848, doi:10.1029/2001JD900049.
- Shapiro, M. A. (1974), A multiple structured frontal zone-jet stream system as revealed by meteorologically instrumented aircraft, *Mon. Weather Rev.*, *102*(3), 244–253.
- Shapiro, M. A. (1978), Further evidence of the mesoscale and turbulent structure of upper level jet stream–frontal zone systems, *Mon. Weather Rev.*, *106*(8), 1100–1111.
- Sherlock, V., A. Hauchecorne, and J. Lenoble (1999), Methodology for the independent calibration of Raman backscatter water-vapor lidar systems, *Appl. Opt.*, *38*(27), 5816–5837.
- Škerlak, B., M. Sprenger, and H. Wernli (2014), A global climatology of stratosphere–troposphere exchange using the ERA-Interim data set from 1979 to 2011, *Atmos. Chem. Phys.*, *14*(2), 913–937.
- Škerlak, B., M. Sprenger, S. Pfahl, E. Tyrlis, and H. Wernli (2015), Tropopause folds in ERA-Interim: Global climatology and relation to extreme weather events, *J. Geophys. Res. Atmos.*, *120*, 4860–4877, doi:10.1002/2014JD022787.
- Sprenger, M., and H. Wernli (2003), A northern hemispheric climatology of cross-tropopause exchange for the ERA15 time period (1979–1993), *J. Geophys. Res.*, *108*(D12), 8521, doi:10.1029/2002JD002636.
- Sprenger, M., M. Croci Maspoli, and H. Wernli (2003), Tropopause folds and cross-tropopause exchange: A global investigation based upon ECMWF analyses for the time period March 2000 to February 2001, *J. Geophys. Res.*, *108*(D12), 8518, doi:10.1029/2002JD002587.
- Sprenger, M., H. Wernli, and M. Bourqui (2007), Stratosphere–troposphere exchange and its relation to potential vorticity streamers and cutoffs near the extratropical tropopause, *J. Atmos. Sci.*, *64*(5), 1587–1602.
- Stevenson, D. S., et al. (2006), Multimodel ensemble simulations of present-day and near-future tropospheric ozone, *J. Geophys. Res.*, *111*, D08301, doi:10.1029/2005JD006338.
- Stevenson, D. S., et al. (2013), Tropospheric ozone changes, radiative forcing and attribution to emissions in the Atmospheric Chemistry and Climate Model Intercomparison Project (ACCMIP), *Atmos. Chem. Phys.*, *13*(6), 3063–3085.
- Stohl, A., and T. Trickl (1999), A textbook example of long-range transport: Simultaneous observation of ozone maxima of stratospheric and North American origin in the free troposphere over Europe, *J. Geophys. Res.*, *104*(D23), 30,445–30,462, doi:10.1029/1999JD900803.
- Stohl, A., M. Hittenberger, and G. Wotawa (1998), Validation of the Lagrangian particle dispersion model FLEXPART against large-scale tracer experiment data, *Atmos. Environ.*, *32*(24), 4245–4264.
- Stohl, A., et al. (2003a), Stratosphere–troposphere exchange: A review, and what we have learned from STACCATO, *J. Geophys. Res.*, *108*(D12), 8516, doi:10.1029/2002JD002490.
- Stohl, A., H. Wernli, P. James, M. Bourqui, C. Forster, M. A. Liniger, P. Seibert, and M. Sprenger (2003b), A new perspective of stratosphere–troposphere exchange, *Bull. Am. Meteorol. Soc.*, *84*(11), 1565–1573.
- Stohl, A., C. Forster, A. Frank, P. Seibert, and G. Wotawa (2005), Technical note: The Lagrangian particle dispersion model FLEXPART version 6.2, *Atmos. Chem. Phys.*, *5*(9), 2461–2474.
- Sutton, R. T., H. Maclean, R. Swinbank, A. O'Neill, and F. W. Taylor (1994), High-resolution stratospheric tracer fields estimated from satellite observations using Lagrangian trajectory calculations, *J. Atmos. Sci.*, *51*(20), 2995–3005.
- Thouret, V., J. Y. N. Cho, R. E. Newell, A. Marengo, and H. G. J. Smit (2000), General characteristics of tropospheric trace constituent layers observed in the MOZAIK program, *J. Geophys. Res.*, *105*(D13), 17,379–17,392, doi:10.1029/2000JD900238.
- Trickl, T., H. Feldmann, H.-J. Kanter, H.-E. Scheel, M. Sprenger, A. Stohl, and H. Wernli (2010), Forecasted deep stratospheric intrusions over Central Europe: Case studies and climatologies, *Atmos. Chem. Phys.*, *10*(2), 499–524.
- Tulet, P., K. Suhre, C. Mari, F. Solmon, and R. Rosset (2002), Mixing of boundary layer and upper tropospheric ozone during a deep convective event over Western Europe, *Atmos. Environ.*, *36*(28), 4491–4501.
- Vaughan, G., J. D. Price, and A. Howells (1994), Transport into the troposphere in a tropopause fold, *Q. J. R. Meteorol. Soc.*, *120*(518), 1085–1103.
- Vogelmann, H., R. Sussmann, T. Trickl, and A. Reichert (2015), Spatiotemporal variability of water vapor investigated using lidar and FTIR vertical soundings above the Zugspitze, *Atmos. Chem. Phys.*, *15*(6), 3135–3148.
- Wang, J., et al. (2010), Water vapor variability and comparisons in the subtropical Pacific from The Observing System Research and Predictability Experiment-Pacific Asian Regional Campaign (T-PARC) Driftsonde, Constellation Observing System for Meteorology, Ionosphere, and Climate (COSMIC), and reanalyses, *J. Geophys. Res.*, *115*, D21108, doi:10.1029/2010JD014494.
- Wernli, B. H., and H. C. Davies (1997), A Lagrangian-based analysis of extratropical cyclones. I: The method and some applications, *Q. J. R. Meteorol. Soc.*, *123*(538), 467–489.
- Wernli, H. (1997), A Lagrangian-based analysis of extratropical cyclones. II: A detailed case-study, *Q. J. R. Meteorol. Soc.*, *123*(542), 1677–1706.
- World Meteorological Organization (1986), Atmospheric ozone 1985, Rep. 20 WMO Global Ozone Res. and Monit. Proj., Geneva, Switz.
- Zanis, P., et al. (2003), Forecast, observation and modelling of a deep stratospheric intrusion event over Europe, *Atmos. Chem. Phys.*, *3*(3), 763–777.
- Zhang, K., R. Fu, T. Wang, and Y. Liu (2016), Impact of geographic variations of the convective and dehydration center on stratospheric water vapor over the Asian monsoon region, *Atmos. Chem. Phys.*, *16*, 7825–7835, doi:10.5194/acp-16-7825-2016.